**Development of high sensitivity materials**

**for applications in magneto-mechanical torque sensor**

by

**Yuping Shen**

A thesis submitted to the graduate faculty

in partial fulfillment of the requirements for the degree of

MASTER OF SCIENCE

Major: Materials Science and Engineering

Program of Study Committee:

David C. Jiles, Major Professor

John E. Snyder

Gary Tuttle

Iowa State University

Ames, Iowa

2003

Graduate College

Iowa State University

This is to certify that the master's thesis of

Yuping Shen

has met the thesis requirements of Iowa State University

David Sires

**Major Professor**

Lawrence J. Genalo

**For the Major Program**

# Table of Contents

## ABSTRACT

The Matteucci effect, which mainly manifests itself as the change of magnetization of a material with torsional stress, is currently of great technological interest because of the search for magnetic torque sensors. Magnetic torque sensors are important to future improvements of automobiles and industrial robots. It is well known that the magnetic state of a material depends on both the external magnetic field and external stress which causes strain and change in magnetization of the material. The former phenomenon has been well understood in both theory and application. However, the magnetic state dependence of stress is not adequately understood and the experimental data is of limited extent.

In this project, the Matteucci effect in iron, cobalt, nickel and permalloy rods has been documented when they were in magnetic remanence status along the axis and nickel ring when they were in remanence status along the circumference. The effect of annealing on the magnetomechanical effect in nickel and the temperature dependence of the magnetomechanical sensitivity has also been examined.

Factors related to the sensitivity at equilibrium condition have been theoretically developed. It is found in the experiments that the mechanism of magnetic domain wall movement plays an important role rather than the domain rotation. A higher sensitivity was found by domain wall movement mechanism than that by domain rotation mechanism. However, the domain wall movement will result in more hysteresis than domain wall rotation.

The dynamic process of Matteucci effect of iron, cobalt, permally, especially as-fabricated and annealed nickel rods have been examined. A tentative explanation for the

difference of these in terms of magnetic domain configuration and domain wall movement was given.

As a result, another method of configuring and processing magnetic domains to get a linear magnetomechanical response other than that suggested by Garshelis, which was the basic method before the present studies, has been experimentally developed and theoretically analyzed. A higher sensitivity was obtained in nickel by employing this method than that by employing the method of Garshelis. The results suggest that magnetic domain configuration is very important in designing a high sensitivity magnetic torque sensor.

**Key words: Matteucci Effect, Magnetomechanical Effect, Magnetic Torque Sensors.**

# Chapter 1. Introduction

## 1.1 Background

Magnetic torque sensors are important to future improvements of automobiles and industrial robots. It has been calculated by automotive manufacturers that the use of electronic steering systems based on magnetoelastic torque sensors will lead immediately to a 5% improvement in automotive fuel efficiency. This is because the hydraulic systems currently in use continuously draw high levels of power, whereas the electronic systems draw lower power and only draw power as needed. The fuel efficiency improvement implies that $3.7\times10^{9}$ gallons of gasoline can be saved every year for US passenger cars alone by using new energy efficient magneto-electronic steering systems. Also, drive shaft sensors can be used to monitor engine misfire in order to control and minimize unwanted and harmful emissions in exhaust. The Matteucci effect [1] is thus currently of great technological interest because of the potential usage in magnetic torque sensors.

The primary advantage of a magnetic torque sensor is that any change of magnetic induction can be conveniently sensed by a Hall effect probe or other magnetic measurement method, such as magnetoresistive (MR) or giant magnetoresistive (GMR) sensors without contacting the shaft subjected to torque. Basically the Matteucci effect manifests itself by the change of magnetization of a material with torsional stress. This can occur both with and without an external applied magnetic field. The literature on this subject has been until recently very limited since Matteucci first discovered the phenomenon in 1847 [1]. This is because, in most cases, the Matteucci effect is non-linear and path dependent (hysteretic) so that its practical application is limited. Research by Garshelis and coworkers [2, 3, 4] has

shown that the development of a magnetoelastic torque sensor is a realistic goal for automotive steering applications. Fig.1.1 shows a torque transducer utilizing a circularly polarized ring that was first suggested by Garshelis in 1992 [2]. Linear variation of field as a function of applied torque was obtained from this transducer. Jiles [5] developed a theory of the magneto-mechanical effect in 1995. Herbst *et al* [6] developed model calculations of torque-induced axial magnetization in circumferentially magnetized rings. However, there is still a long way to go before this type of transducer can be introduced to routine engineering practice. First, the sensitivity, which is defined as the change of detected signal with applied torque, is too low for materials such as iron and steel to be useful in applications. Chen et al [7] developed this type of torque sensor utilizing a new material, specifically a metal-bonded cobalt ferrite composite which has large magnetoelastic coefficients. A large magneto-mechanical sensitivity has been observed in metal-bonded cobalt ferrite composite. Second, magnetomechanical effects of some materials were experimentally found to give relatively large magnetomechanical hysteresis at room temperature. However, cobalt ferrite composites show very good hysteresis-free response only above 60 $^{\circ}$C as shown in Fig.1.2. In addition to high sensitivity, low hysteresis should be another key consideration for improving material properties for magnetic torque sensors. However, in the previous literature, little attention has been paid to this issue. Third, the sensitivity should be as stable as possible when the sample is subjected to different loads and temperatures. Again, very little work has been focused on this area.

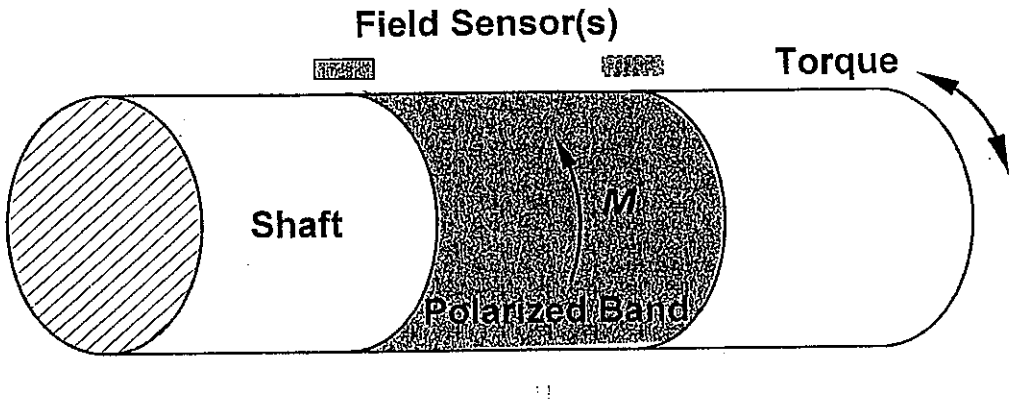


**Fig.1.1** A torque transducer utilizing a circularly polarized ring. First presented by Garshelis [2].

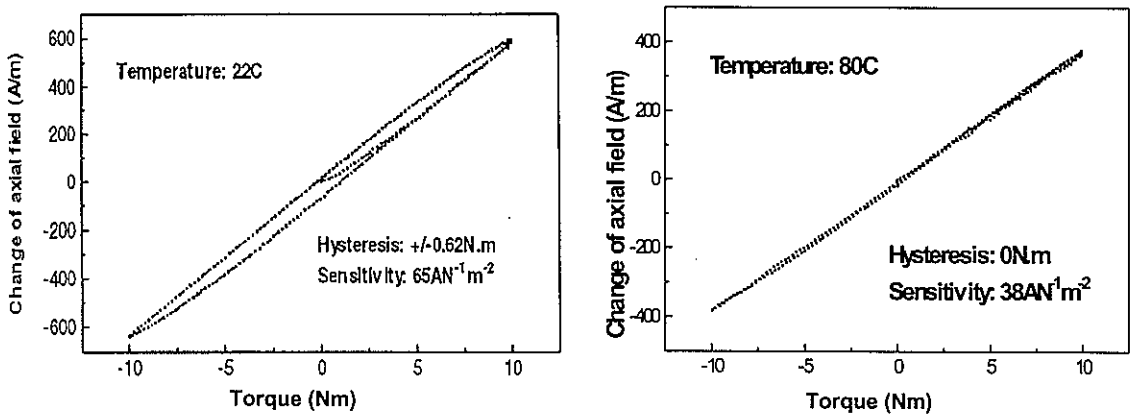


**Fig. 1.2** The magneto-mechanical torque response of cobalt ferrite at 22 °C and 80 °C. After Chen *et al* [7].

## 1.2 Scope of this work

Nickel, iron, cobalt and nickel-iron alloys in the form of cylindrical rods have been used to examine the Matteucci effect. This series of materials has advantages because they contain different magnetostriction constants and magnetic anisotropy constants. They provide rich information of how magnetostriction and magnetic anisotropy affect the Matteucci effect. Also, they all have large elastic moduli and elastic limits that make them resilient against strong torque compared to other materials. Pure torque will load the rod samples and cause the magnetic induction to change along the surface which can be recorded by a Hall sensor. The research in this thesis covers the following aspects in detail.

1. Investigation of the Matteucci effect in nickel rods with different configurations of magnetic domains.
2. Investigation of how internal stress affects the Matteucci effect in nickel. Nickel rods with the same dimensions were fabricated in the same condition. One half of them were selected for annealing at 500 $^{\circ}$C for 2 hours to reduce their internal stress. Matteucci effects of these two types of samples were compared in both domain configurations mentioned above.
3. The Matteucci effect in a series of compositions of iron nickel alloy as well as iron, nickel and cobalt have been examined. This series of compositions includes $Fe_{64}Ni_{36}$, $Fe_{55}Ni_{45}$ and $Fe_{10}Ni_{90}$. These have different intrinsic properties such as different magnetostriction coefficients and different magnetic anisotropy constants.
4. The sensitivity change of polycrystalline nickel samples versus different temperature have been investigated to provide the basic information of the stability of the sensitivity with temperature.

# Chapter 2. Theory of Elasticity

## 2.1 Load, direct stress and direct strain

External force applied to a body in equilibrium results in internal forces being set up within the materials. If a cylindrical bar is subjected to a pull or push along its axis as shown in Fig.2.1, then it is said to be subjected to load, either in tension or compression. The unit of load is measured in newtons. If the tension or compression is uniformly or equally applied across the cross-section, the internal forces set up are also distributed uniformly and the bar is said to be subjected to a uniform *direct stress*. The stress is defined as:

$$stress(\sigma) = \frac{load}{area} = \frac{F}{A} \tag{2.1}$$

When the bar is subjected to a stress, the bar will change in length. Let the original length of the bar be L and the changes in length be $\delta l$, the strain produced is defined as follows [9]:

$$strain(\varepsilon) = \frac{change\ \ in\ \ length}{original\ \ length} = \frac{\delta l}{L} \tag{2.2}$$

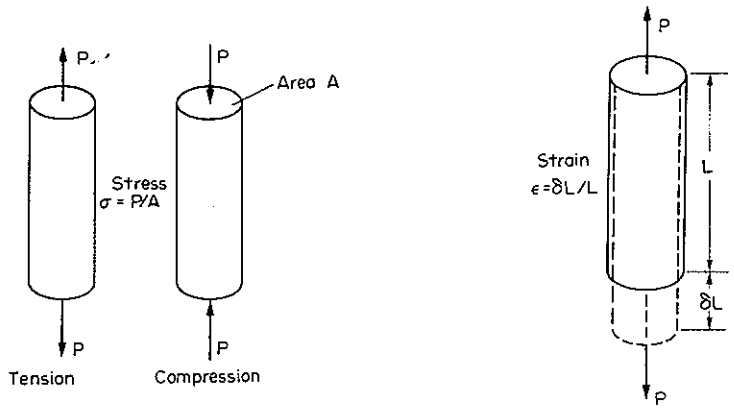


**Fig.2.1** (a) Types of direct stress. (b) Strain under load. After E.J. Hearn [9].

Strain is a measure of the deformation of the material and is dimensionless. For mathematical convenience, tensile stresses and strains are considered positive in sense; compressive stresses and strains are considered negative in sense.

**2.2 Elastic materials, modulus of elasticity and Hooke's law**

A material is said to be elastically deformed if it returns to its original, unloaded dimensions when the load is removed. In practice, strain is found to be proportional to the stress within a load limit known as the elastic limit. Hooke's law states that, within the elastic limit,

$$stress(\sigma) \propto strain(\varepsilon)$$

or

$$\frac{stress}{strain} = constant \tag{2.3}$$

This constant is given the symbol $E$ and termed the modulus of elasticity. Thus for axial stress and axial strain,

$$E = \frac{stress}{strain} = \frac{\sigma}{\varepsilon} = \frac{F/A}{\delta L/L} = \frac{FL}{A\delta L} \tag{2.4}$$

Modulus of elasticity of a material is generally assumed to be the same in tension or compression and for most engineering materials has a numerical value of the order of 10's to 100's of GPa. Table 2.1 lists the typical values of Young's modulus of basic ferromagnetic materials iron, cobalt and nickel.

**Table 2.1** Young's modulus and modulus of rigidity of iron, cobalt and nickel. Data are cited from reference [10, 11, 12, 13]

| | Iron | Cobalt | Nickel |
|---|---|---|---|
| Elastic Modulus (GPa) | 190 | 211 | 210 |
| Shear Modulus (GPa) | 75 | 82.6 | 80 |
| Poisson's ratio | 0.3 | 0.32 | 0.31 |

## 2.3 Shear stress, shear strain and modulus of rigidity

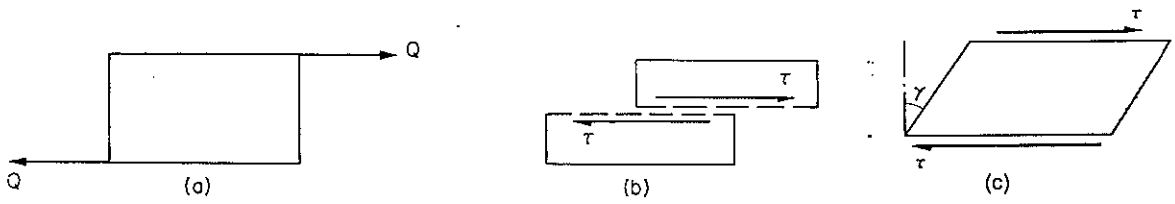


**Fig. 2.2 (a)** Shear force **(b)** resulting shear strain showing typical form of failure by relative sliding of planes. **(c)** Shear strain produced by shear stress. After Hearn [9].

Consider a block or portion of material as shown in Fig. 2.2 (a) subjected to a pair of equal and opposite forces Q. There is then a tendency for one layer of the material to slide over another to produce the form of strain shown in Fig. 2.2 (b). A shear stress τ is set up, defined as follows:

$$shear \quad stress(\tau) = \frac{shear \quad load}{area \quad resisting \quad shear} = \frac{F}{A} \qquad (2.5)$$

This shear stress will always be tangential to the area on which it acts; longitudinal stress, however, is always normal to the area on which it acts. The block will change shape or "strain" into the form shown in Fig 2.2 (c) The angle of deformation $\gamma$ is termed the shear strain. Shear strain is measured in radians and hence is dimensionless. For materials within the elastic range the shear strain is proportional to the shear stress producing it, i.e.

$$\frac{shear\ \ stress}{shear\ \ strain} = \frac{\tau}{\gamma} = constant = G \qquad (2.6)$$

the constant G is termed the modulus of rigidity or shear modulus and is analogous to the modulus of elasticity used in the longitudinal stress application. The data of Young's modulus and modulus of rigidity of iron, cobalt and nickel are listed in Table 2.1.

## 2.4 Principal stress and principal axes

To fully describe the state of material interaction at any given point in a body, nine components of stress are necessary of which six are independent if the examined body is in equilibrium [14].

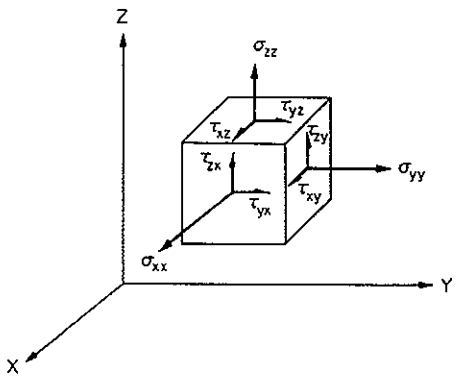


**Fig 2.3** Nine components of stress fully descript the state of stress of an element.

These nine components of stress form a symmetric matrix when in equilibrium.

$$\sigma = \begin{pmatrix} \sigma_{11} & \tau_{12} & \tau_{13} \\ \tau_{21} & \sigma_{22} & \tau_{23} \\ \tau_{31} & \tau_{32} & \sigma_{33} \end{pmatrix} \qquad (\tau_{ij}=\tau_{ji}), \tag{2.7}$$

According to matrix theory, for a symmetric matrix, a set of coordinates can be found with respect to which the matrix of stress components can be reduced to a diagonal matrix of the form

$$\sigma = \begin{pmatrix} \sigma_1 & 0 & 0 \\ 0 & \sigma_2 & 0 \\ 0 & 0 & \sigma_3 \end{pmatrix} . \tag{2.8}$$

The particular set of coordinate axes with respect to which the stress matrix is diagonal are called the principal axes, and the corresponding stress components are the principal stresses. Physically, each of the principal stresses is normal on a principal plane, and there is no shear component on that plane.

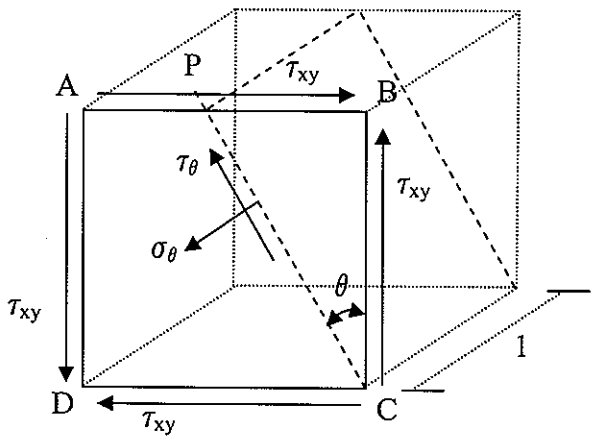


**Fig. 2.4** Stress on an element subjected to pure shear.

One would now like to examine the principal axes of a circular rod under pure shear. Consider the element shown in Fig 2.4 to which shear stresses have been applied to the sides

AB and DC. Complementary shear stresses of equal value but of opposite effect are necessary on sides AD and BC in order to prevent rotation of the element when in equilibrium. Since the applied and complementary shears are of equal value on the x and y planes, they are both given the symbol $\tau_{xy}$. Consider now the equilibrium of portion PBC. Resolving normal to PC assuming unit length,

$$\sigma_\theta |PC| = \tau_{xy}|BC|\sin\theta + \tau_{xy}|PB|\cos\theta = \tau_{xy}|PC|\cos\theta\sin\theta + \tau_{xy}|PC|\sin\theta\cos\theta \qquad (2.9)$$

Simplifying the equation, we get

$$\sigma_\theta = \tau_{xy}\sin 2\theta \qquad (2.10)$$

Similarly, resolving forces parallel to PC,

$$\tau_\theta |PC|1 = \tau_{xy}|PB|\sin\theta - \tau_{xy}|BC|\cos\theta = \tau_{xy}|PC|\sin^2\theta - \tau_{xy}|PC|\cos^2\theta \qquad (2.11)$$

Simplifying the equation, we get

$$\tau_\theta = -\tau_{xy}\cos 2\theta \qquad (2.12)$$

When $\theta=45^0$, $\tau_\theta$ reaches zero while $\sigma_\theta$ reaches the maximum of $\tau_{xy}$. When $\theta=-45^\circ$, $\tau_\theta$ reaches another zero while $\sigma_\theta$ reaches the value of $-\tau_{xy}$.

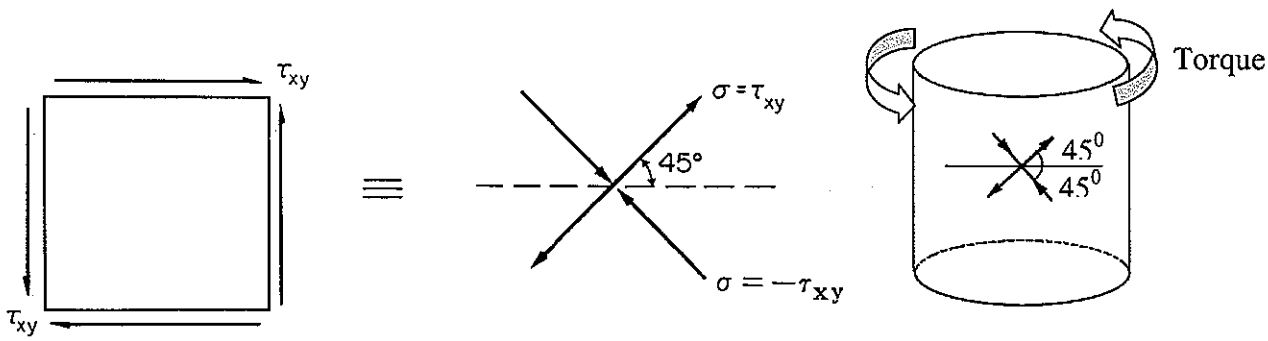


**Fig. 2.5** Direct stress due to pure torque.

Therefore the system of pure shear stresses produces a pair of equivalent direct stresses as shown in Fig 2.5, one compressive stress and one tensile stress, each at 45° to the original shear directions, and equal in magnitude to the applied shear.

**2.5 Stress strain relationship**

In the previous section, we showed that the nine component stresses can be reduced to 3 independent direct stresses by selecting a particular set of coordinates. Experiments show that stress along a particular direction not only causes strain along that direction, but also causes strain along other perpendicular directions. Say, principal stress $\sigma_x$ causes a positive strain $\varepsilon_x$ along the x direction. It also causes a complementary negative strain of $-\varepsilon_y$, $-\varepsilon_z$ along the y axis and the z axis respectively. In practice, the quotients of $\varepsilon_y/\varepsilon_x$ and $\varepsilon_z/\varepsilon_x$ are found to be a constant for isotropic polycrystalline material. It is termed the Poisson's coefficient $\nu$. Thus the stress strain relationship can be expressed as follows for isotropic material:

$$\begin{cases} \varepsilon_x = \frac{1}{E}\left(\sigma_x - \nu(\sigma_y + \sigma_z)\right) \\ \varepsilon_y = \frac{1}{E}\left(\sigma_y - \nu(\sigma_z + \sigma_x)\right) \\ \varepsilon_z = \frac{1}{E}\left(\sigma_z - \nu(\sigma_x + \sigma_y)\right) \end{cases}, \qquad (2.13)$$

The Poisson's coefficient $\nu$ is usually found to be in the range 0.3-0.5.

## 2.6 Simple torsion theory

Consider a solid circular shaft of radius R subjected to a torque at one end with the other end being fixed (Fig. 2.6). Under the action of this torque a radial line at the free end of the shaft twists through an angle $\theta$, point A moves to B, and AB subtends an angle $\gamma$ at the fixed end.

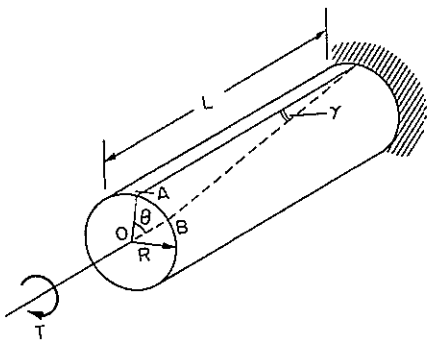


**Fig. 2.6** A rod under pure torque [9].

This is then the angle of distortion of the shaft, i.e. the shear strain.

arc $AB=R\theta=L\gamma$, *and therefore*

$$\gamma=R\theta/L, \tag{2.14}$$

From the definition of modulus of rigidity,

$$\textit{shear strain } \gamma = \textit{shear stress } \tau / G, \tag{2.15}$$

where $\tau$ is the shear stress set up at radius R. Therefore equating above equations gives,

$$\frac{R\theta}{L}=\frac{\tau}{G}$$

$$\frac{\tau}{R}=\frac{G\theta}{L}=\left(\frac{\tau'}{r}\right) \qquad \text{or} \qquad \tau'=\frac{G\theta}{L}r=G\gamma \tag{2.16}$$

where $\tau'$ is the shear stress at any radius $r$. These equations indicate that the shear stress and shear strain vary linearly with radius and have their maximum values at the outside radius as shown in Fig 2.7. It is noticeable that the applied shear stresses in the plane of the cross-section are accompanied by complementary stresses of equal value on longitudinal planes as indicated in Fig 2.7. Some materials of cylindrical shape have different stress limits along the axis and the circumference. Therefore the lower one should take effect when consider the stress limit.

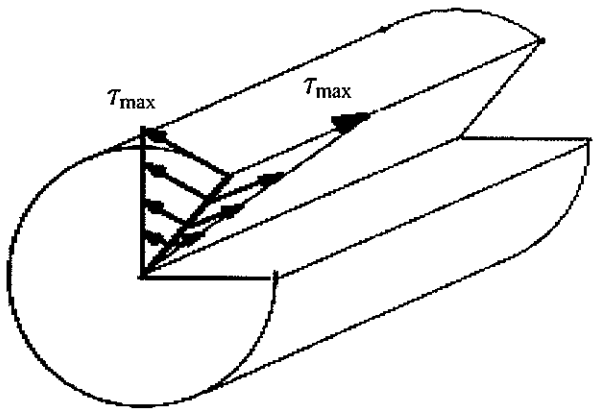


**Fig. 2.7.** Complementary longitudinal shear stress in a shaft subjected to torsion

We now consider how the total torque relates to the shear modulus and twist angle. Let the cross-section of the shaft be considered as divided into elements of radius $r$ and thickness $dr$ as shown in fig.2.8 each subjected to a shear stress $\tau'$.

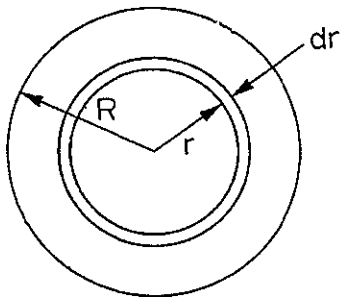


**Fig. 2.8.** Cross-section of a shaft

The torque set up on each element is *stress* × *area* × *radius* . i.e.

$$T = \tau' 2\pi r dr r = 2\pi\tau' r^2 dr . \tag{2.17}$$

the total torque T on section will then be the sum of all such contributions across the section, i.e.

$$T = \int_0^R 2\pi\tau' r^2 dr . \tag{2.18}$$

Now the shear stress $\tau'$ will vary with the radius r and must therefore be replaced in terms of $r$ before the integral is evaluated. Substitute $\tau' = \frac{G\theta}{L} r$ into above equation, we have

$$T = \int_0^R 2\pi \frac{G\theta}{L} r^3 dr = \frac{G\theta}{L} \int_0^R 2\pi r^3 dr = \frac{G\theta}{L} \frac{\pi R^4}{2} = \tau_{max} \frac{\pi R^3}{2} \quad \text{or}$$

$$\tau_{max} = \frac{2}{\pi R^3} T \ . \tag{2.19}$$

This is the relationship of the total applied torque T and the reacted maximum torsional stress $\tau_{max}$ . For example, when a torque of $1\ N \bullet m$ was applied to a nickel cylinder of diameter of 13mm, the corresponding torsional stress along the outer circumference is

$$\tau_{max} = \frac{2}{\pi(0.0065)^3} = 2.3MPa \ . \tag{2.20}$$

# Chapter 3. Elements of Magnetism

## 3.1 Origin of magnetism

Ampère first suggested that magnetism in materials originates from equivalent current loops inside a material [15, page 7,14]. The main idea was that when electrical charge is in motion, it produces a magnetic field. The basic mathematical entity of Ampère's theory is an equivalent current loop, as shown in Fig. 3.1. There is a magnetic moment $\bar{m}$ associated with this loop which is equal to the product of the current $\bar{i}$ and the area of the loop $\bar{A}$.

An alternative model of the origin of magnetism in materials is that it arises from magnetic dipole. This contends that there are 2 types of magnetic poles, positive and negative, which are analogous to the positive and negative electric charges. The magnetic poles produce a magnetic field just like the electric charge produces electric field. On the basis of this model a magnetic pole pair, positive and negative, always appears together and forms a magnetic dipole. Until now scientists have not yet found a single magnetic pole or "monopole". The basic mathematical entity of this theory is therefore the magnetic dipole as shown in Fig. 3.1. There is a magnetic moment $\bar{m}$ associated with this dipole which equals to the product of the pole strength $\bar{p}$ and the separation $\vec{l}$ between the poles.

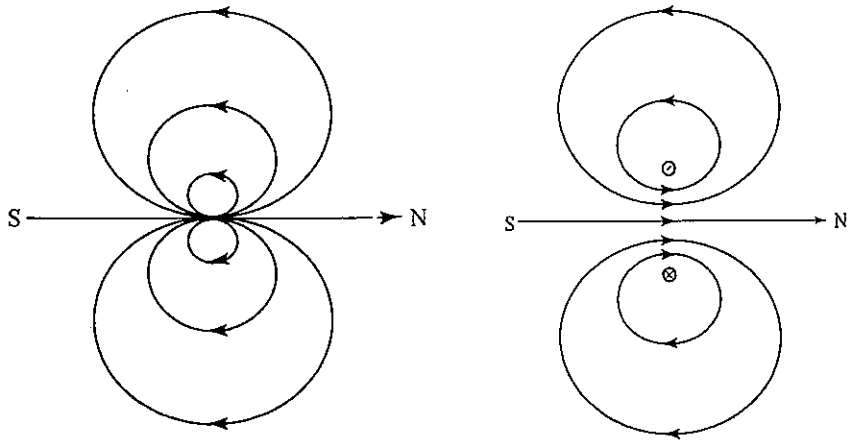


(a) (b)

**Fig. 3.1** Configurations of the most basic mathematical entities. (a) the magnetic dipole and (b) the current loop (after Cullity).

To say a magnetic source exists, it must be evidenced by the effect on other trial objects. When the distance between the magnetic source and the trial object is much larger than the separation between the poles, both models of the origin of magnetism (current loops or poles) are the same for the effect on other objects [15, 16]. Thus both current loop and magnetic dipole are mathematically equivalent entities on a macroscopic scale. This provides us alternative options to explain macroscopic magnetic phenomena.

### 3.2 Magnetic field *H*, Magnetization *M*, magnetic induction *B* and demagnetization factor $N_d$

As stated in the previous section, a current loop or a magnetic dipole with magnetic moment $\vec{m}$ causes magnetic field in the space near it. To measure this effect, the magnetic field can be defined as follows:

*In the vacuum or free space, for an infinitely long wire, if the current passing through it is 1 amp, the magnitude of magnetic field at a radial distance of 1 m is* $\frac{1}{2\pi}$ *amp / meter; the direction of the magnetic field is defined by* $\vec{i} \times \vec{r}$, *where* $\vec{i}$ *is the unit vector of current,* $\vec{r}$ *is the unit vector of the position from the radius.*

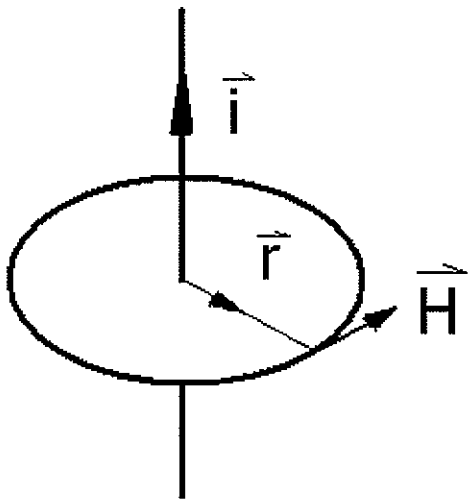


**Fig. 3.2** Definition of magnetic field generated by an infinitely long wire in vacuum.

The general calculation of magnetic field in macroscopic situations is given by Biot-Savart law or Ampère's circuital law. The Biot-Savart law states that

$$\delta\vec{H} = \frac{1}{4\pi r^2} i\delta\vec{l} \times \vec{u} \qquad (3.1)$$

where $i$ is the current flowing in an elemental length $\delta l$ of a conductor, r is the radial distance, u is a unit vector along the radial direction and $\delta H$ is the contribution to the magnetic field at r due to the current element $i\delta l$. Ampère's circuital law states that

$$i = \oint Hdl \qquad (3.2)$$

where $i$ is the algebraic sum of the current that are enclosed by the integrated closed path. Biot-Savart law and Ampère's circuital law are equivalent when calculating the magnetic field generated by a current source in vacuum space.

Consider a volume $V$ that contains $N$ magnetic moments $\vec{m}$. Magnetization $\vec{M}$ is defined as,

$$\vec{M} = \frac{\sum \vec{m}}{V} \tag{3.3}$$

or if all $\boldsymbol{m}$ are aligned along the same direction,

$$\vec{M} = \frac{N\vec{m}}{V} \tag{3.4}$$

Let's consider the magnetic field $\vec{H}_{source}$ within the volume $V$ generated by these N magnetic sources.

$$\vec{H}_{source} = f(\vec{M}) \tag{3.5}$$

If this volume V includes a position that an external group of magnetic sources generate a magnetic field of $\boldsymbol{H_{ex}}$ at that point for vacuum space, the total magnetic field within the volume V is given by

$$\vec{H}_{in} = \vec{H}_{ex} + \vec{H}_{source} = \vec{H}_{ex} + f(\vec{M}) \tag{3.6}$$

where $H_{ex}$ is the applied external magnetic field. $H_{source}$ is the magnetic field generated by the sample itself. The average magnetic field at a position within the volume V is given by the sum of the contributions to the magnetic field by all the magnetic moments $\boldsymbol{m}$. The magnetic field generated by the source can be approximately expressed as:

$$H_{source} = M - N_d M \ , \tag{3.7}$$

where $N_d$ is a coefficient greater than 0 and less than 1 and is termed as demagnetization factor. It is noticeable that in SI unit the magnetic field and the magnetization are in the same units.

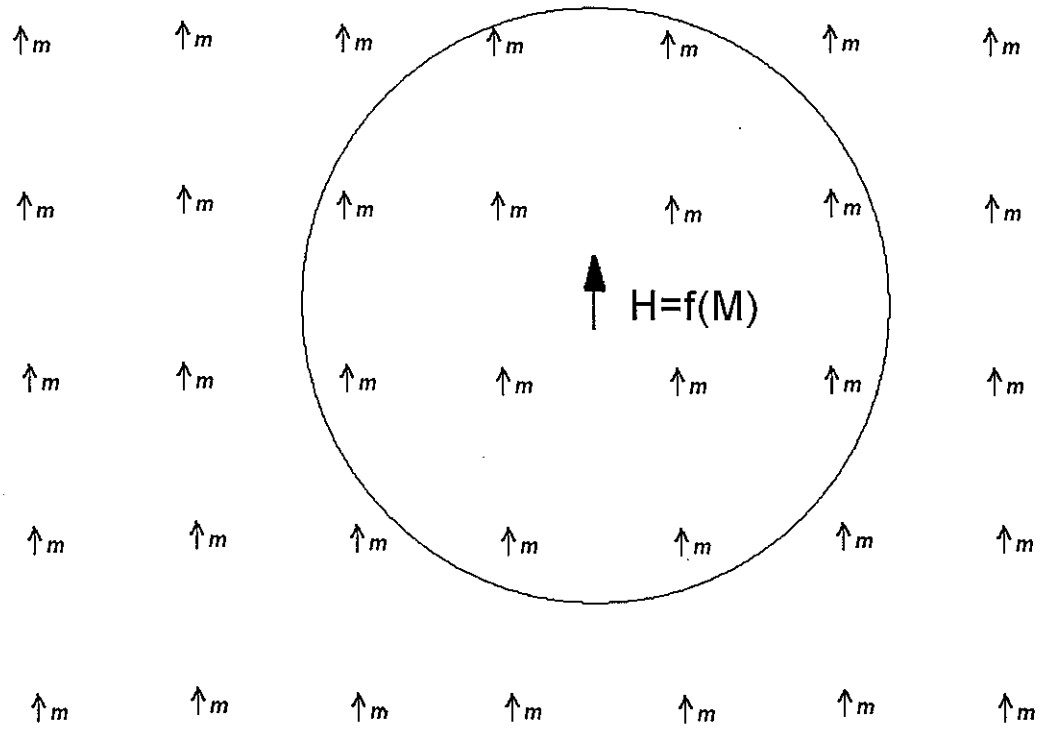


**Fig.3.3** Magnetic field generated by the magnetic sources themselves within the magnetic sources with a volume V.

Thus the total magnetic induction within the magnetic sources is given by,

$$B_{in} = \mu_0(H_{in} + M) = \mu_0 H_{ex} + \mu_0 H_{source} + \mu_0 M = \mu_0 H_{ex} + \mu_0 f(M) + \mu_0 M \qquad (3.8)$$

Experiments show when a magnetic moment is subject to a magnetic field, torque may be exerted on the magnetic moment. The maximum torque generated by the magnetic field is found to be

$$T_{\max} = \mu_0 \bar{m} \times \bar{H}_{total} \qquad (3.9)$$

where $\mu_0$ is a constant and has the value of $4\pi \times 10^{-7} Nm/(A^2 m^{-2}) = 4\pi \times 10^{-7} Hm^{-1}$. The term $\mu_0 H_{total}$ is defined as magnetic induction $\boldsymbol{B}$. Thus, for position where the demagnetization field is 0, one gets

$$\vec{B} = \mu_0 \vec{H}_{total} = \mu_0 (\vec{H}_{ex} + \vec{M}) \tag{3.10}$$

When we mention magnetic field, it usually refers to the applied magnetic field $\vec{H}_{ex}$; when we mention magnetic induction, it refers to the effect of total magnetic field $\mu_0 H_{total}$ as $\vec{B} = \mu_0 \vec{H}_{total}$. Magnetic induction is also called magnetic flux density.

Magnetization $\boldsymbol{M}$ of a sample is usually dependent on the external magnetic field $\vec{H}_{ex}$ which is the cause of changes in the alignment of the magnetic moments $\boldsymbol{m}$ and thus alters the vector summation of $\boldsymbol{m}$ which when divided by volume $V$ determines the value of magnetization $\boldsymbol{M}$.

### 3.3 Maxwell's equations of the electromagnetic field

Maxwell combined and integrated the work of previous investigators in electromagnetic fields and formulated four differential equations [15] that set up the basis of classical electromagnetism. These are

$$\nabla \times H = J + \frac{\partial D}{\partial t} \qquad \text{(Ampère's law)} \tag{3.11}$$

$$\nabla \times E = -\frac{\partial B}{\partial t} \qquad \text{(Faraday's law)} \tag{3.12}$$

$$\nabla \bullet B = 0 \qquad \text{(Gauss's magnetic flux law)} \tag{3.13}$$

$$\nabla \bullet D = \rho \qquad \text{(Gauss's electric flux law)} \tag{3.14}$$

where $\boldsymbol{E}$ is the electric field, $\boldsymbol{D}$ the electric flux density, $\boldsymbol{J}$ the current density and $\rho$ the charge density. It is noticeable that all of these equations were obtained as a result of macroscopic observation.

# Chapter 4. Magnetic Anisotropy and Magnetostriction

Magnetic properties of magnetic materials usually depend on the direction in which they are measured [15, 16]. This phenomenon is called magnetic anisotropy. There are two kinds of anisotropy:

1. Intrinsic anisotropy. Also called crystal anisotropy or magnetocrystalline anisotropy.
2. Extrinsic anisotropy. Also called induced anisotropy. This may be caused by many factors such as shape, stress, magnetic annealing or plastic deformation.

Although the physical origin of magnetocrystal anisotropy is rooted in quantum theory, it is customary to describe the anisotropy of a crystal by macroscopic coefficients $K_1$, $K_2$ that are obtained using a phenomenological analysis. This is because the calculation of crystal anisotropy from quantum theory is complex and usually $K_1$, $K_2$ are enough to give the required information on crystal anisotropy in a given material.

## 4.1 Anisotropy in Cubic Crystals

For a cubic single crystal, measurements of magnetization curves along different crystallographic directions give different results. The results for iron, which has a body-centered cubic structure, and nickel, which has a face-centered cubic structure, are shown in Fig. 4.1(a) and Fig. 4.1(b) respectively. For iron, these measurements show that saturation can be achieved with the lowest field strength in <100> direction. Thus <100> is accordingly called the "easy direction" of magnetization. For nickel, the easy direction is found to be the <111> direction.

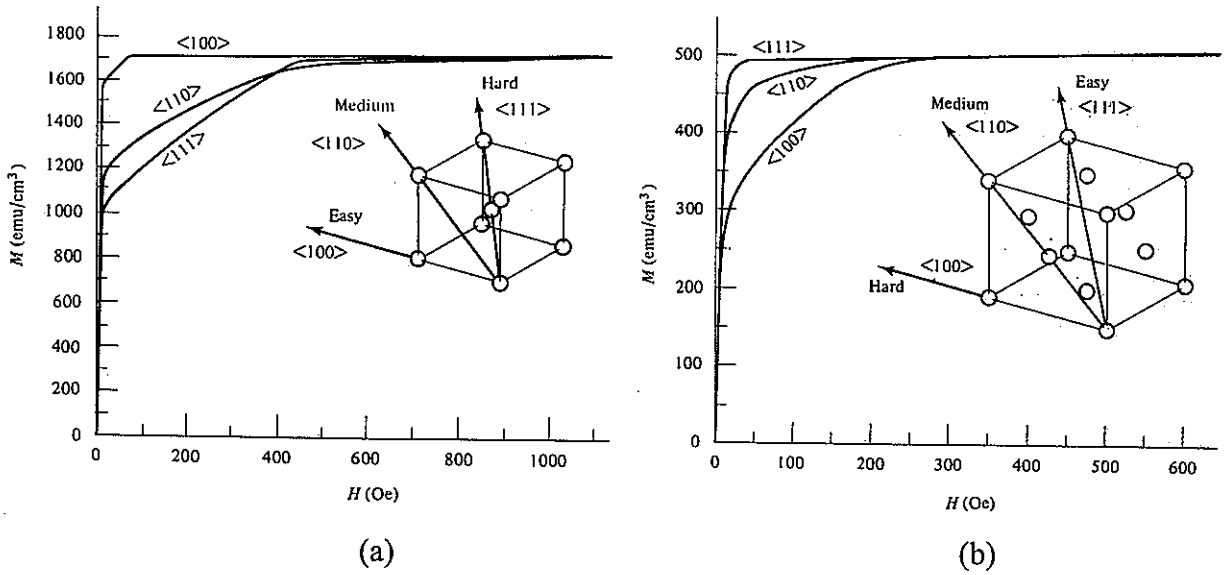


**Fig. 4.1** Magnetization curves for single crystals of (a) iron, and (b) nickel. After Cullity[16].

From these figures, the areas enclosed between the magnetization curve and the M axis, which corresponds to the energy needed to saturate the magnetization, are different along different directions. An easy direction thus can be considered as the direction along which the lowest energy will be needed to magnetize the sample to saturation. More generally, the direction of easy magnetization of a crystal is the direction of spontaneous domain magnetization in the zero field demagnetized state. Because the applied field must do work against the anisotropy force in order to turn the magnetization vector away from an easy direction, there must be additional energy stored in any crystal in which $M_s$ points in a noneasy direction. This is called the crystal anisotropy energy $E_a$. Akulov [17] showed that the crystal anisotropy energy $E_a$ can be expressed in terms of a series expansion of the direction cosines of $M_s$ relative to the crystal. For a cubic crystal, let $\theta_1, \theta_2, \theta_3$ be the angles of $M_s$ relative to the crystal axes, and $\alpha_1, \alpha_2, \alpha_3$ be the cosines of these angles. Because of the

symmetry of a cubic crystal, the crystal anisotropy energy should have the following properties.

(1) Any interchange of $\theta_1, \theta_2, \theta_3$, thus any interchange of $\alpha_1, \alpha_2, \alpha_3$ does not change the environment of $M_s$, and thus does not change the value of anisotropy energy $E_a$

(2) Inversion of $M_s$ compared with the original direction does not change the environment of $M_s$. Therefore, $E(\theta_1, \theta_2, \theta_3)=E(\theta_1+\pi, \theta_2+\pi, \theta_3+\pi)$; thus $E(\alpha_1, \alpha_2, \alpha_3)= E(-\alpha_1, -\alpha_2, -\alpha_3)$;

(3) Rotation of $M_s$ with respect to any axes for $180^0$ does not change the environment of $M_s$. For example, if we rotate $M_s$ with respect to $z$ axes for $180^0$, the new angles of $M_s$ relative to the crystal axes are $\theta_1+\pi, \theta_2+\pi, \theta_3$. Therefore, in conjunction with property (2) we obtain, $E(\alpha_1, \alpha_2, \alpha_3)= E(\alpha_1, \alpha_2, -\alpha_3)= E(\alpha_1, -\alpha_2, \alpha_3)= E(-\alpha_1, \alpha_2, \alpha_3)$.

According to these properties, the series expansion of $E_a$ can not contain any odd power of $\alpha_1, \alpha_2, \alpha_3$. Expanding $E_a$ in terms of the direction cosines $\alpha_1, \alpha_2, \alpha_3$, the expression must have the form

$$E = A_0 + A_1\sum_{i=1}^{3}\alpha_i^2 + A_2\sum_{\substack{i,j \\ i\neq j}}\alpha_i^2\alpha_j^2 + A_3\sum_{i=1}^{3}\alpha_i^4 + A_4\alpha_1^2\alpha_2^2\alpha_3^2 + A_5\sum_{\substack{i,j \\ i\neq j}}\alpha_i^4\alpha_j^2 + A_6\sum_{i}\alpha_i^6 + \ldots \tag{4.1}$$

where $A_i$'s are constants. Bearing in mind that $\alpha_1^2+\alpha_2^2+\alpha_3^3=1$. We have

$$\sum_{i=1}^{3}\alpha_1^2 = 1 \tag{4.2}$$

$$\sum_{i=1}^{3}\alpha_i^4 = (\sum_{i=1}^{3}\alpha_i^2)^2 + 2\sum_{\substack{i,j \\ i\neq j}}\alpha_i^2\alpha_j^2 = 1 + 2\sum_{\substack{i,j \\ i\neq j}}\alpha_i^2\alpha_j^2 \tag{4.3}$$

$$\sum_{\substack{i,j \\ i\neq j}} \alpha_i^{\,4}\alpha_j^{\,2} = \frac{1}{2}\left(\sum_{\substack{i,j \\ i\neq j}} \alpha_i^{\,2}\alpha_j^{\,2} - 3\alpha_1^{\,2}\alpha_2^{\,2}\alpha_3^{\,2}\right) \tag{4.4}$$

$$\sum_{i=1}^{3} \alpha_i^{\,6} = \sum_{i=1}^{3} \alpha_i^{\,4} - 2\sum_{\substack{i,j \\ i\neq j}} \alpha_i^{\,4}\alpha_j^{\,2} = 1 + \sum_{\substack{i,j \\ i\neq j}} \alpha_i^{\,2}\alpha_j^{\,2} + 3\alpha_1^{\,2}\alpha_2^{\,2}\alpha_3^{\,2} \tag{4.5}$$

Substituting equations (4.2), (4.3) and (4.4) into the equation (4.1), we have

$$E_a = (A_0 + A_1 + 2) + (A_2 + 3\frac{1}{2})\sum \alpha_i^{\,2}\alpha_j^{\,2} + (A_4 + \frac{3}{2})\alpha_1^{\,2}\alpha_2^{\,2}\alpha_3^{\,2} + \ldots \tag{4.6}$$

Rewriting the above equation, one gets

$$E_a = K_0 + K_1(\alpha_1^{\,2}\alpha_2^{\,2} + \alpha_2^{\,2}\alpha_3^{\,2} + \alpha_3^{\,2}\alpha_1^{\,2}) + K_2(\alpha_1^{\,2}\alpha_2^{\,2}\alpha_3^{\,2}) + \ldots \tag{4.7}$$

where $K_0$, $K_1$, $K_2$,...are the anisotropy coefficients for a particular material and are expressed in Joules/m$^3$. Higher powers are generally not needed, and sometimes even $K_2$ is so small that the term involving it can be neglected. The first term, which is simply $K_0$, is independent of angle and is usually ignored, because normally we are interested only in the change in the energy $E_a$ when the $M_s$ vector rotates from one direction to another.

When $K_2$ is zero, the direction of easy magnetization is determined by the sign of $K_1$. If $K_1$ is positive, then $E_{100}<E_{110}<E_{111}$, and consequently <100> is the easy direction, because $E_a$ is the minimum when $M_s$ is in that direction. Iron and the cubic ferrites containing cobalt have positive values of $K_1$. If $K_1$ is negative, $E_{111}<E_{110}<E_{100}$, and consequently <111> is the easy direction. $K_1$ is negative for nickel and the cubic ferrites that contain no cobalt.

When $K_2$ is not zero, the easy direction is determined by the values of both $K_1$ and $K_2$. The way in which the values of these two constants determine the directions of easy, medium, and hard magnetization is shown in Table 4.1. The room temperature anisotropy constants of several ferromagnetic materials are listed in Table 4.2.

**Table 4.1** Directions of easy, medium, and hard magnetization in a cubic crystal. After Cullity [16 ].

| $K_1$ | + | + | + | - | - | - |
|---|---|---|---|---|---|---|
| $K_2$ | $+\infty$ to $-9K_1/4$ | $-9K_1/4$ to $-9K_1$ | $-9K_1$ to $-\infty$ | $-\infty$ to 9 $\|K_1\|/4$ | $9\|K_1\|/4$ to 9 $\|K_1\|$ | $9\|K_1\|$ to $+\infty$ |
| Easy | <100> | <100> | <111> | <111> | <110> | <110> |
| Medium | <110> | <111> | <100> | <110> | <111> | <100> |
| Hard | <111> | <110> | <110> | <100> | <100> | <111> |

**Table 4.2** Crystalline anisotropy constants of different materials.

| Structure | Substance | $K_1(10^3$ J/m$^3)$ | $K_2(10^3$ J/m$^3)$ |
|---|---|---|---|
| Cubic | Fe | 48.1 | 12 |
| | Ni | -5.48 | -2.47 |
| | $FeO \bullet Fe_2O_3$ | -11.8 | -28 |
| | $CoO \bullet Fe_2O_3$ | 270 | 300 |
| | $NiO \bullet Fe_2O_3$ | -7.0 | - |
| | $MnO \bullet Fe_2O_3$ | -3.79 | 0 |
| | $Mn_{0.45}Zn_{0.55}Fe_2O_4$ | -0.62 | - |
| | $Mn_{0.52}Zn_{0.40}Fe_{2.08}O_4$ | -0.10 | - |
| | $CuFe_2O_4$ | -6.3 | - |
| | $MgFe_2O_4$ | -3.75 | - |
| Hexagonal | Co | 412 | 143 |
| | $BaO \bullet 6Fe_2O_3$ | 330 | - |
| | $2CoO \bullet BaO \bullet 8Fe_2O_3$ | -186 | 75 |
| | $2CoO \bullet 3BaO \bullet 12Fe_2O_3$ | -180 | - |

**4.2 Anisotropy in hexagonal crystals**

Cobalt has a hexagonal close-packed structure. The hexagonal axis c is the easy direction of magnetization, and, within the accuracy of the measurements, any direction in the basal plane is found to be approximately equally hard, meaning that there is little anisotropy within the basal plane. Therefore, the anisotropy energy $E_a$ depends on only a single angle, the angle θ between the $M_s$ vector and the c axis. According to the crystalline symmetry, the anisotropy energy under these circumstances is given by:

$$E_a = K_0' + K_1' \cos^2\theta + K_2' \cos^4\theta + \ldots \qquad (4.8)$$

However, it is customary to write the equation for $E_a$ in hexagonal crystals in powers of $\sin\theta$. Bearing in mind that $\cos^2\theta = 1 - \sin^2\theta$, we get

$$E_a = K_0 + K_1 \sin^2\theta + K_2 \sin^4\theta + \ldots \qquad (4.9)$$

When $K_1$ is positive and $K_2 > -K_1$, the energy $E_a$ is a minimum for $\theta = 0°$, and the c axis is along the easy magnetization direction, as in cobalt. Under this circumstance, the crystal is referred to as one with a "uniaxial anisotropy". The energy $E_a$ will have a minimum for $\theta = 90°$ if $K_1$ is negative and $K_2 < |K_1|/2$. The basal plane is then an easy plane of magnetization and the material is referred to as one with a "basal plane anisotropy". If $K_1$ is negative and $K_2 > |K_1|/2$, then $E_a$ is minimum for $\theta = \sin^{-1}(-K_1 / 2K_2)^{1/2}$. The $M_s$ vector may lie anywhere on the surface of a cone with a semi vertex angle of $\theta$.

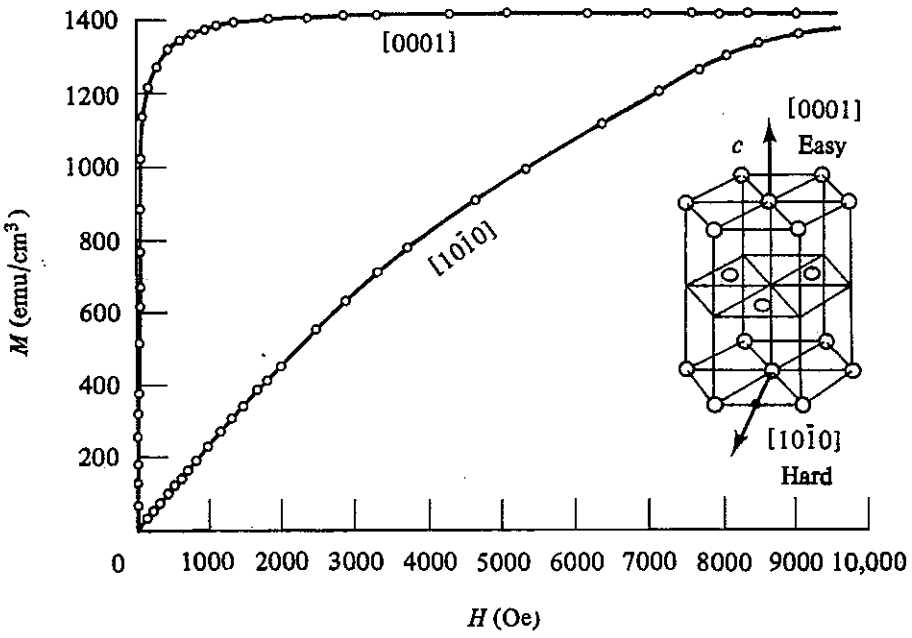


**Fig. 4.2** Magnetization curves of a single crystal of cobalt. After Cullity [16 ].

### 4.3 Physical Origin of Crystal Anisotropy

We now consider the physical origin of crystal anisotropy. Magnetic order such as ferromagnetism originates from exchange interaction between electrons. From the point of view of quantum theory, Heinsenberg suggested that the ordering of local magnetization arises from the exchange energy $E_{ex}$ of electron pairs.

$$E_{ex} = J\sum_{i,j} \bar{S}_i \bullet \bar{S}_j \tag{4.10}$$

where $J$ is the constant of exchange integration, $\bar{S}_i$, $\bar{S}_j$ are the quantum spin vectors of two interacting electrons. It is customary to divide the motion of electron into spin and orbit. For a single free atom, both spin and orbit magnetic moments of electrons contribute the total

magnetic moment. In a crystal, atoms are fixed at the lattice points. Thus an electron is not only subject to the Coulomb force of the nucleus that it rotates around and other electrons of the atom, but also subject to the Coulomb force by other nuclei and their electrons.

The effect of other nuclei and their electrons is called the crystal field. Crystal field lowers the symmetry of the environment of electrons. This lowered symmetry leads to a split of the energy degeneracy of the orbital component of moment. The split causes the orbital magnetic moment to be "quenched"—the orbital magnetic moments cancel each other. We call this the orbit-lattice coupling. The orbit-lattice coupling is very strong so that even a strong external magnetic field can not affect the "quenched" orbit magnetic moment. This means the orbital magnetic moment are fixed strongly to the lattice. Since the orbital magnetic moment is "quenched", it does not affect the magnetocrystalline anisotropy.

We call the exchange interaction between the two neighboring spins "spin-spin" coupling. In ferromagnetism or anti-ferromagnetism this coupling is strong so that it keeps neighboring spins aligned, either parallel or anti-parallel respectively. However, the spin-spin coupling depends to a first approximation only on the angle between adjacent spins, not on the crystalline axes. Therefore, spin-spin coupling does not contribute to magnetocrystalline anisotropy.

There is also a coupling between the spin and the orbit motion of an electron known as "spin-orbit" coupling. When an external magnetic field is applied, it tries to reorient the direction of electron's spin and hence the orbital motion because of the spin-orbit coupling. However the orbital motion direction is strongly constrained by the lattice. So the spin-orbit coupling tries to resist the reorientation of the spin direction. The energy that is needed to overcome the spin-orbit coupling to rotate the spin magnetic moment of a domain from the

easy direction is the anisotropy energy. This coupling is relatively weak compared with the other coupling energies because fields of a magnitude of $10^5$ A/m are usually enough to rotate the spin such as iron or nickel from the easy direction.

### 4.4 Magnetomechanical effect.

The elastic properties of a solid body can be characterized by a unique expression connecting the components of stress and strain at any point in the body for most materials. For some materials, however, especially the ferromagnetic metals and their alloys, the strain is also a function of the external magnetic field in which the body is placed. The state of magnetization of such a body also depends not only on the magnetic field but also on the stress components as shown in Fig 4.3.

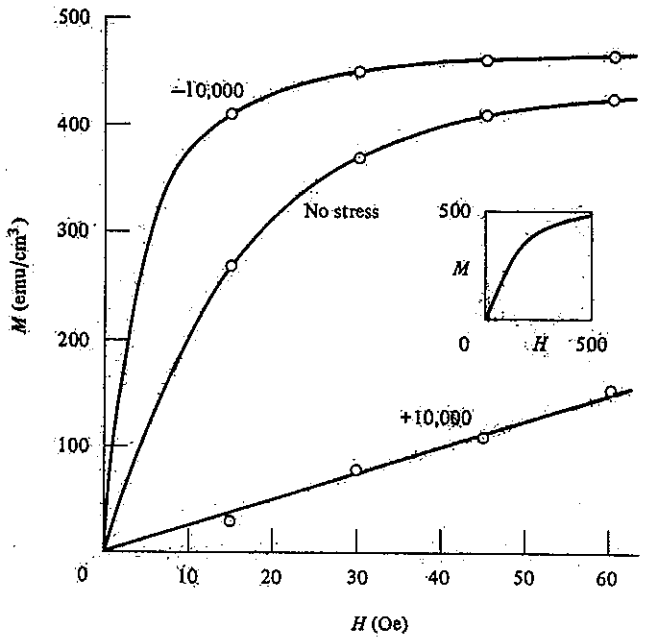


**Fig. 4.3** Effects of applied tensile (+) and compressive (-) stress on the magnetization of nickel. Numbers on curves are stresses in lb/in$^2$. Inset: behavior of nickel under 10,000 lb/in$^2$ tension at higher fields. After Cullity [16].

The elastic and magnetic states of the body are thus interdependent and each is a function both of the applied field and of the applied stress. When external stress is absent, we call the strain from applied magnetic field magnetostriction. When stress is incorporated, we call this case the magnetomechanical effect. Only in recent years have models of the magnetomechanical effect been disclosed [5, 18-21]. The most challenging problem is to describe the hysteretic behavior of ferromagnetic materials under both magnetic field and stress since both reversible and irreversible magnetic domain movement involved. Jiles [5] presented a model which simulates the hysteresis under stress.

**4.5 Magnetostriction.**

In the case of magnetostriction, the state of magnetization and the state of strain of ferromagnetic materials are both dependent only on the external magnetic field. In practice, it is also found that at the Curie temperature, both magnetization and elastic properties show anomalies. That means the elastic and magnetic states of a ferromagnetic material are physically rooted in the same atomic level theory. Nevertheless the empirical magneto-elastic coupling expressions are accurate enough for most materials applications.

It is reasonable to suppose that the strain totally depends on the magnetocrystalline anisotropy when a ferromagnetic material subject to external magnetic field. i.e. there exists spontaneous strain for each magnetic domain. If the magnetic domain is capable of being strained homogeneously along any direction, it requires that the magnetic field within the magnetic domain is the same for all points. Only an ellipsoid can produce a uniform demagnetizing field inside the sample. Therefore within individual homogeneous domains

the strain varies with angle $\theta$ from the direction of spontaneous magnetization according to the relation, as shown in Fig 4.4.

$$e(\theta) = e\cos^2\theta \tag{4.11}$$

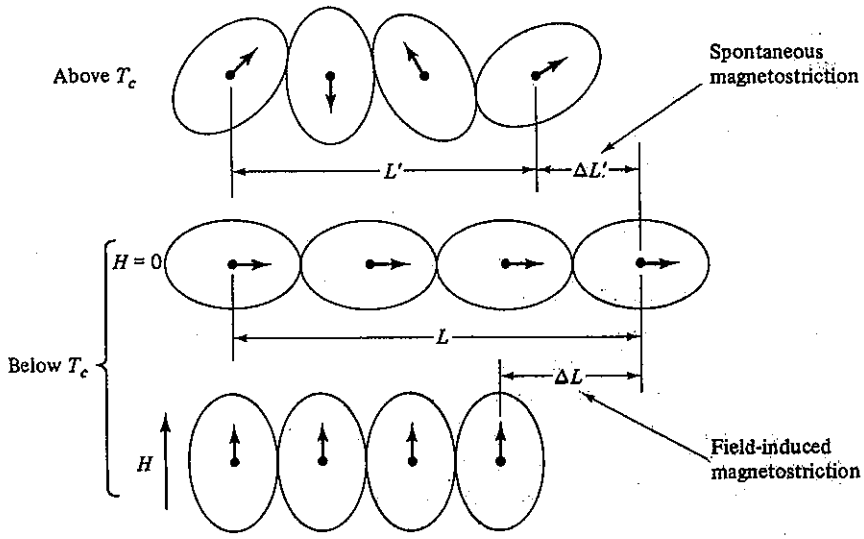


**Fig. 4.4.** Mechanism of magnetostriction [After Jiles].

Based on this model, polycrystalline ferromagnetic material, the expression for the magnetostriction has been developed for cubic crystalline anisotropy as [15]

$$\frac{dl}{l} = \frac{3}{2}\left(\alpha_1^2\beta_1^2 + \alpha_2^2\beta_2^2 + \alpha_3^2\beta_3^2 - \frac{1}{3}\right) + 3\lambda_{111}\left(\alpha_1\alpha_2\beta_1\beta_2 + \alpha_2\alpha_3\beta_2\beta_3 + \alpha_3\alpha_1\beta_3\beta_1\right) \tag{4.12}$$

where $\alpha_1$, $\alpha_2$, $\alpha_3$ are the direction cosines of the magnetization and the three crystalline axis. $\beta_1$, $\beta_2$, $\beta_3$ are the direction cosines of the strain measured related to original coordinate axes.

If a further approximation is made, say $\lambda_{100} = \lambda_{111} = \lambda_s$, where $\lambda_{100}$, $\lambda_{111}$ and $\lambda s$ are the magnetostriction constant along [100], magnetostriction constant along [111] and saturation magnetostriction constant, respectively, equation (4.11) reduces to

$$\frac{dl}{l} = \frac{3}{2}\lambda_s\left(\cos^2\theta - \frac{1}{3}\right) \tag{4.12}$$

where $\theta$ is the angle between the magnetization and the direction of measurement. For randomly oriented (i.e. untextured) polycrystals, it is found $\lambda_s = \frac{2}{5}\lambda_{100} + \frac{3}{5}\lambda_{111}$. The magnetoelastic constants for some ferromagnetic materials are listed in table 4.3

**Table 4.3** Magneto-striction constants of some substance.

| | $\lambda_{100}$ ($10^{-6}$) | $\lambda_{111}$ ($10^{-6}$) | $\lambda_s = \frac{2}{5}\lambda_{100} + \frac{3}{5}\lambda_{111}$ ($10^{-6}$) |
|---|---|---|---|
| Fe | 21 | -21 | -4 |
| Ni | -46 | -24 | -33 |
| Fe-Ni (85%Ni) | -3 | -3 | -3 |
| Fe-Co(40%Co) | 146.6 | 8.7 | 64 |
| $Fe_3O_4$ | -20 | 78 | 39 |
| $Co_{0.8}Fe_{2.2}O_4$ | -590 | +120 | -164 |
| $Mn_{0.8}Co_{0.3}Fe_{2.0}O_4$ | -200 | 65 | -40 |
| $Zn_{0.3}Co_{0.2}Fe_{2.2}O_4$ | -210 | 110 | -18 |
| Terfenol | 90 | 1640 | 1020 |

## Chapter 5. Experiments and Procedure

The materials that were examined included nickel, iron and nickel-iron alloy (permalloy) rods with dimensions of Φ13mm×70mm. These rods were fabricated with a 6x6x13 mm rectangular shaft at each end of the sample for loading torque. The dimension of the samples is shown in Fig 5.1. One half of the as-fabricated nickel rods were selected for annealing at 500 °C for 2 hours to examine the effects of annealing.

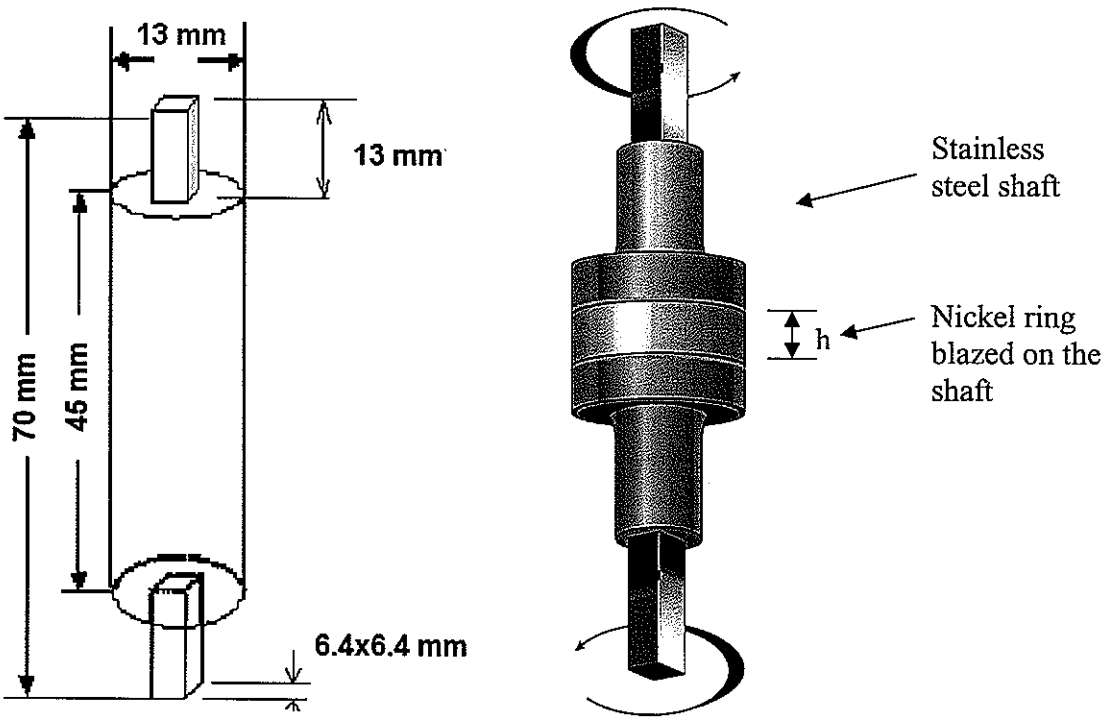


**Fig.5.1** Geometry of samples.

Nickel toroid samples were also studied. The dimensions of the shaft of each sides of the nickel rings are the same of those of nickel rod. The height h (Fig. 5.1) of the nickel rings ranged from 8 to 20 cm.

All samples were magnetized to saturation and left in remanence status before running the test. There were two types of magnetizing procedures. The first method was to magnetize the sample along the axis to saturation by a solenoid. This method was applied to all iron, cobalt, nickel and permalloy rod samples. The second method was to magnetize the sample along the circumference and keep them at remanent status. This was achieved by rotating the sample at a high speed in a slowly decreasing gradient magnetic field generated by a yoked electromagnet. The second method was applied to nickel ring samples.

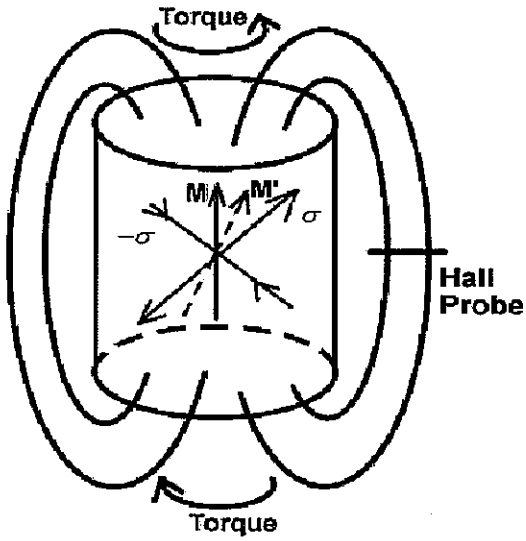


**Fig. 5.2** Schematic of experiment setup.

After magnetizing along the cylinder axis, the as-cast rods were divided into two groups to examine the dependence of magnetization on direction of stress. One group was initially subjected to applied torque in a clockwise direction; the other was initially subjected to applied torque in a counterclockwise direction. Both were cycled over 25 times. The schematic of the experiment setup was drawn in Fig. 5.2.

A magnetic torque sensor test bed was used as a part of this investigation. It can provide a pure torque on the samples without bending. The accuracy of the applied torque by a computer feedback mechanism was $\pm 0.1$ Nm. A photograph of the test bed is shown in Fig 5.3. The strength of the magnetic field at the sample surface was measured using a Hall effect sensor with an accuracy of $\pm 0.8 Am^{-1}$.

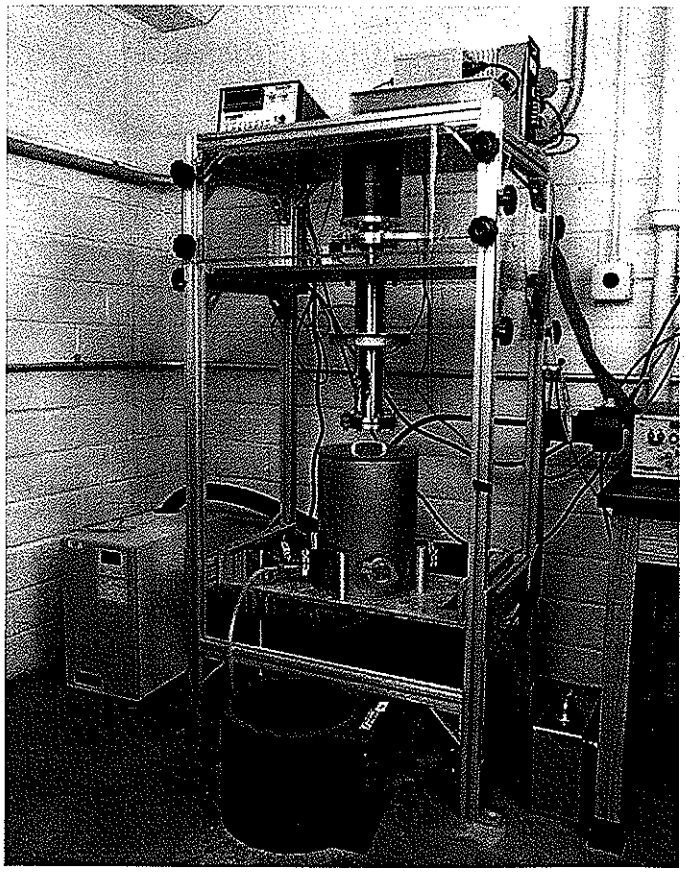

**Fig. 5.3** Magnetic torque sensor test bed.

The samples tested are listed in Table 5.1.

**Table 5.1.** Composition of samples tested.

| Name | Iron | Cobalt | Nickel | Permalloy (in wt%) | | |
|---|---|---|---|---|---|---|
| Composition | 99.9% Fe | 99.9% Co | 99.9% Ni | 99%$Fe_{10}Ni_{90}$ + 1%$Al_2O_3$ | 99%$Fe_{55}Ni_{45}$ + 1%$Al_2O_3$ | 99%$Fe_{66}Ni_{36}$ + 1%$Al_2O_3$ |
| Shape | Rod | Rod | Rod Ring | Rod | Rod | Rod |

# Chapter 6: Experimental Results

## 6.1 Magnetomechanical effect in iron

The magnetomechanical response of iron is shown in Fig.6.1. The rod was initially magnetized along the axis to keep it in remanence status and a Hall sensor was used to measure the magnetic field along the axis. It can be seen that when the torque was under 1Nm, the stress almost does not affect the magnetization. Above that, the surface magnetic field decreased as applied torque increased. After ten cycles of torque, an approximately linear reversible response was obtained. However the sensitivity, which is defined as the quotient of the change of surface magnetic field to applied torque, was as low as 0.1 (A/m)/(Nm).

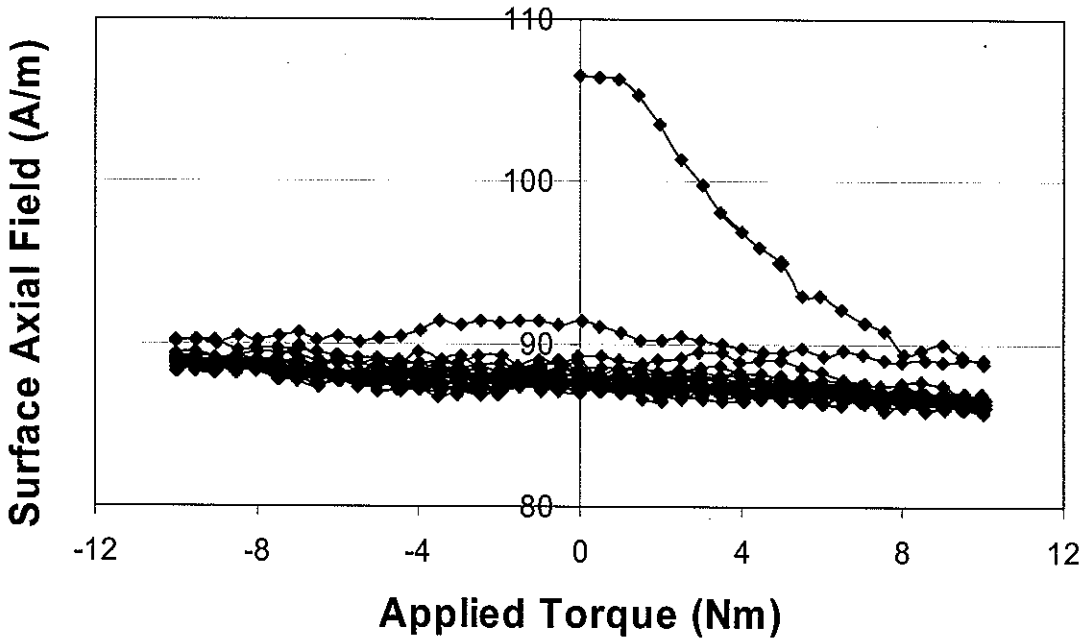


**Fig. 6.1** The magnetomechanical response of a pure iron rod. The rod was initially magnetized along the axis and a Hall sensor was used to measure the surface magnetic field along the axis.

### 6.2 Magnetomechanical effect in cobalt

The magnetomechanical response of a cobalt rod is shown in Fig. 6.2. The rod was initially magnetized along the axis and a Hall sensor was used to measure the surface magnetic field along the axis. The change of the surface axial field is no more than 1% (about 5A/m) and no trend of linearity shown within the range of the applied torque.

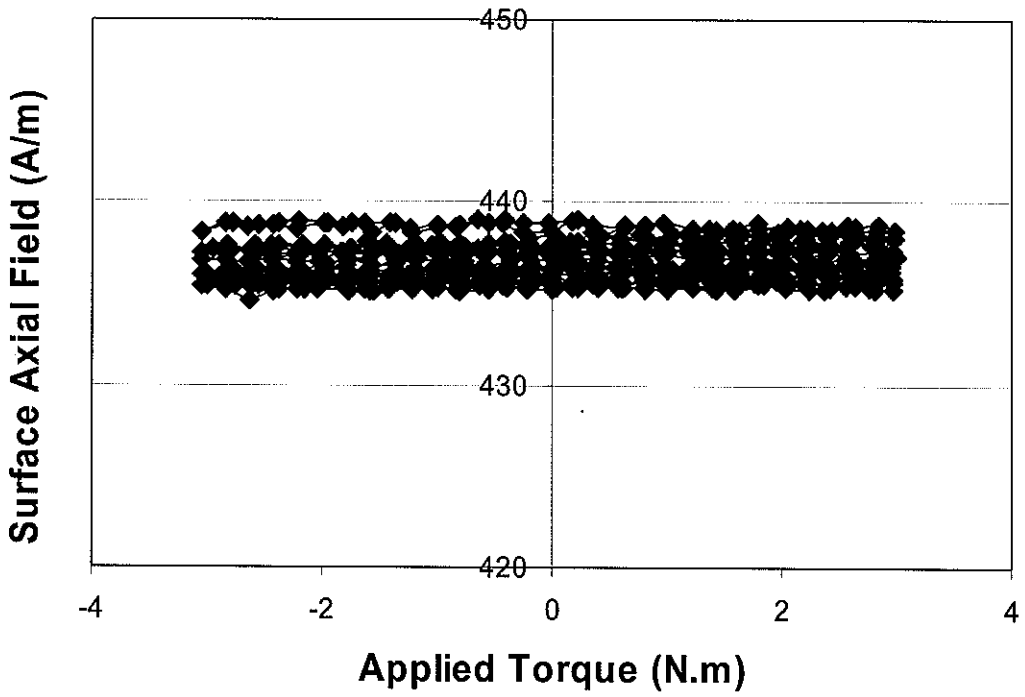


**Fig. 6.2** Magnetomechanical response of a cobalt rod.

### 6.3 Magnetomechanical effect in nickel

Experimental data of as fabricated nickel rods are shown in Fig 6.3. The samples had been magnetized along the axis to saturation and then kept in the remanence status before running the test. Chen [8] has done some measurements of the magnetomechanical effect in nickel and a linear response after 10 cycles of torque was reported. In our experiment, it was

found that the response of the surface magnetic induction along the axis depends on the direction of the initial torque.

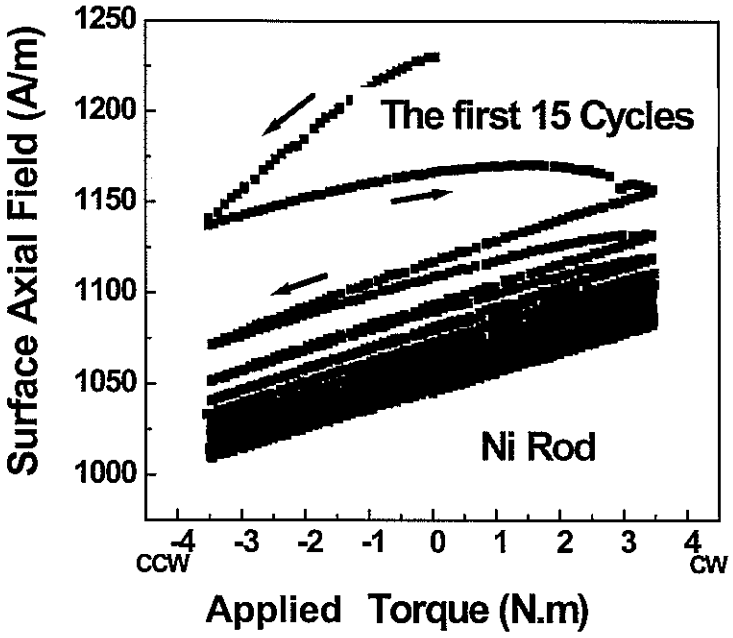


(a)

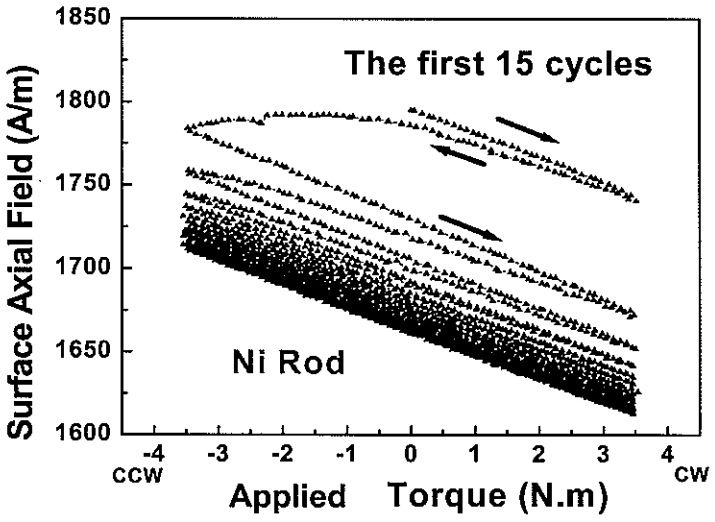


(b)

**Fig. 6.3** As-fabricated nickel rod under torque with (a) initial counter-clockwise direction; and (b) initial clockwise direction.

Fig. 6.4 shows the change in remanent induction of a nickel rod when it was under tensile or compressive stress along the axis. A coil was wounded on the rod to obtain the change of magnetic induction B. During the measurement, a constant stress was applied to the rod on an Instron mechanical test system. Hysteresis was measured in situ. Within the range of applied stress (<25MPa), the remanence was found to be proportional to stress. This range of applied stress is much more than that of the decomposed stress (< 8.1 MPa, in chapter 7.2) when we applied torque on the rods.

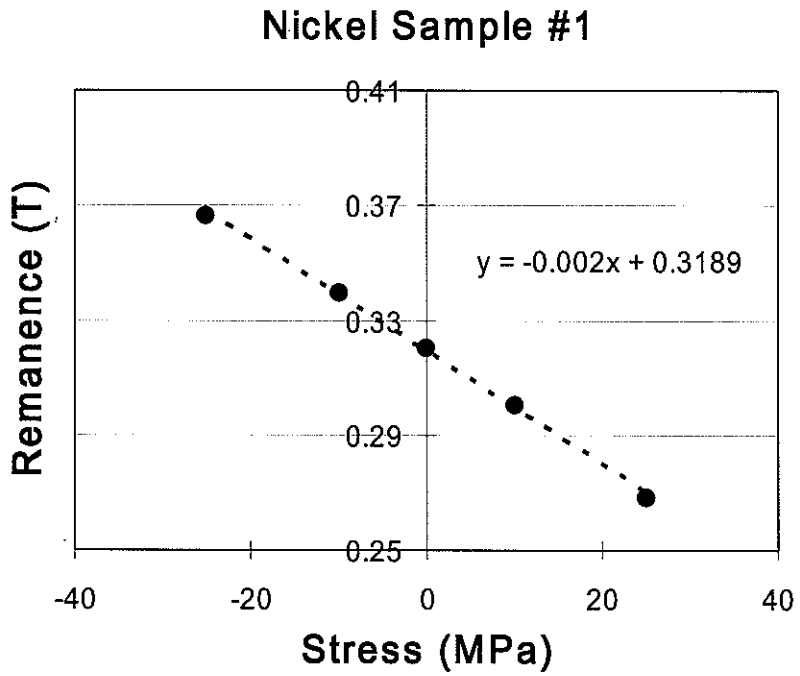


**Fig. 6.4** The change in remanent induction of a nickel rod when it is under tensile or compressive stress along the axis.

Fig. 6.5 shows the temperature dependence of sensitivity (change in surface axial field per $N \bullet m$ of applied torque) of one of as-fabricated nickel rods after 15 cycles of torque. The rod was initially magnetized to saturation along the cylindrical axis. After 20

cycles of applied torque from -3.5 Nm to 3.5 Nm, the sensitivity became stable at room temperature. Then both the sample and the Hall sensor were emerged in a vessel which contains selected composition of water-ethanol liquid. The temperature is controlled from -25 °C to 90 °C. The temperature effect on the response of Hall sensor was eliminated from the raw data.

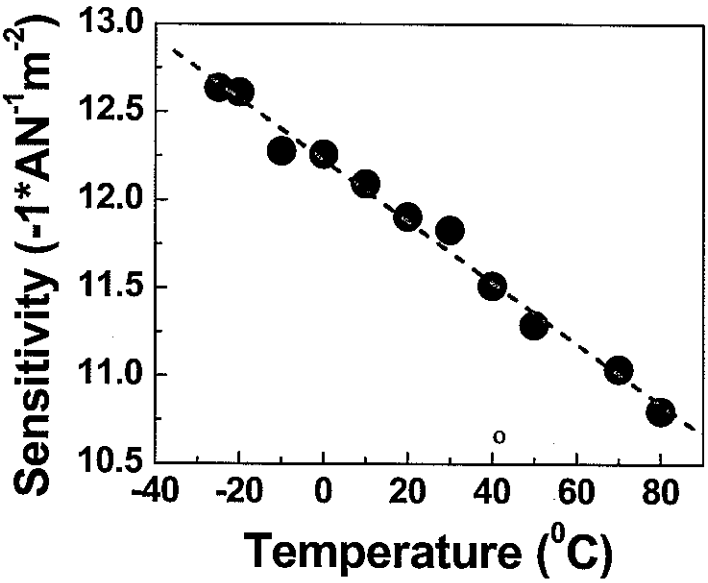


**Fig. 6.5** Temperature dependence of sensitivity of nickel rod after 15 cycles of torque.

The nickel samples annealed at 500 °C have different magnetomechanical response from the as-fabricated samples as shown in Fig. 6.6. It can be seen that the surface axial field of the annealed sample is no longer linear with torque even after many torque cycles. As a comparison, the magnetomechanical response after 15 cycles of both as-fabricated and annealed samples is shown in Fig. 6.7.

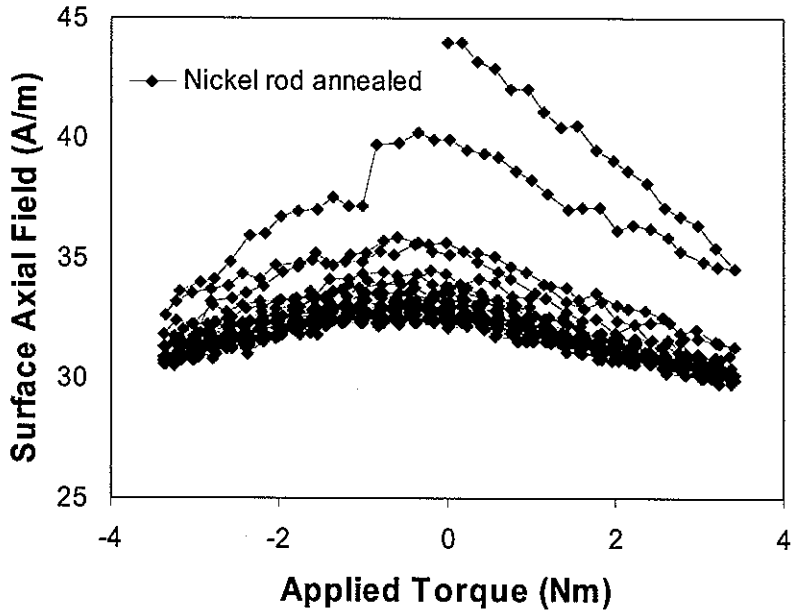


**Fig. 6.6** Matteucci effect of an annealed nickel rod. The rod was initially magnetized along the axis to get remanent status and a Hall sensor was used to measure the magnetic field along the axis.

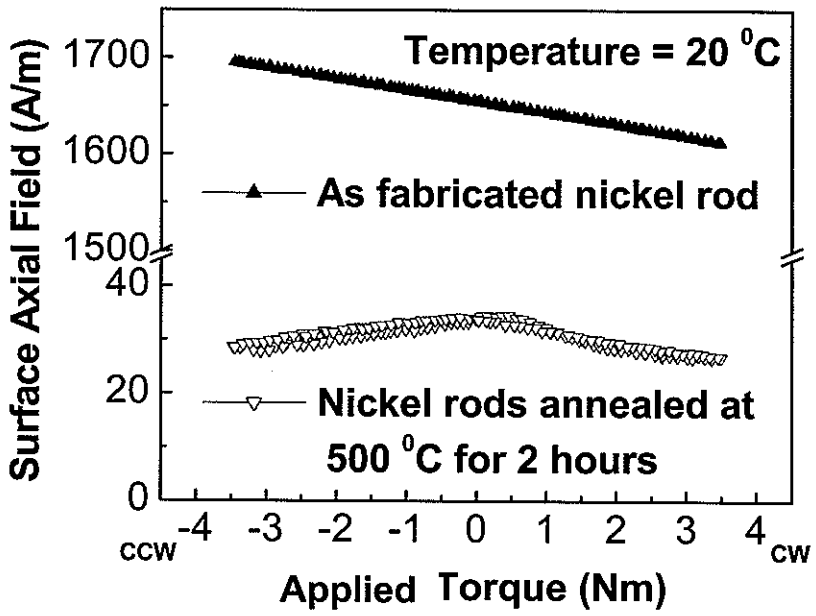


**Fig. 6.7** Magnetomechanical response of as-fabricated nickel rod and nickel rods annealed at 500 °C for 2 hours. This plot is drawn after about 10 cycles of torque.

Matteucci effect of a nickel ring was drawn as Fig. 6.8. The ring was initially magnetized along the circumference and a Hall sensor was used to measure the magnetic induction along the axis. The obtained sensitivity (4.7(A/m)/(Nm)) is much lower than that of as-fabricated nickel rod (31(A/m)/(Nm)) shown in Fig 6.7.

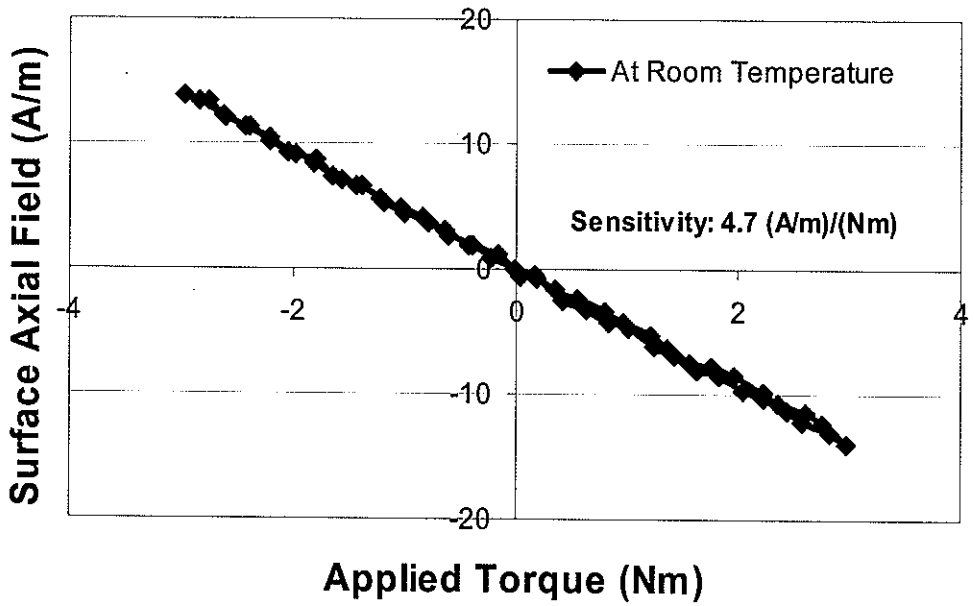


**Fig. 6.8** Matteucci effect of a nickel ring. The rod was initially magnetized along the circumference to get the remanence status. A Hall sensor was used to measure the magnetic field along the axis.

### 6.4 Magnetomechanical effect in permalloy

To examine the magneto-mechanical response of permalloy, we bought samples with 3 different compositions. These were $Fe_{64}Ni_{36}$, $Fi_{55}Ni_{45}$ and $Fe_{10}Ni_{90}$ atomic%. The rods were magnetized along the axis to obtain remanence status before any test. The magneto-mechanical responses are shown in Fig. 6.8, Fig. 6.9 and Fig. 6.10.

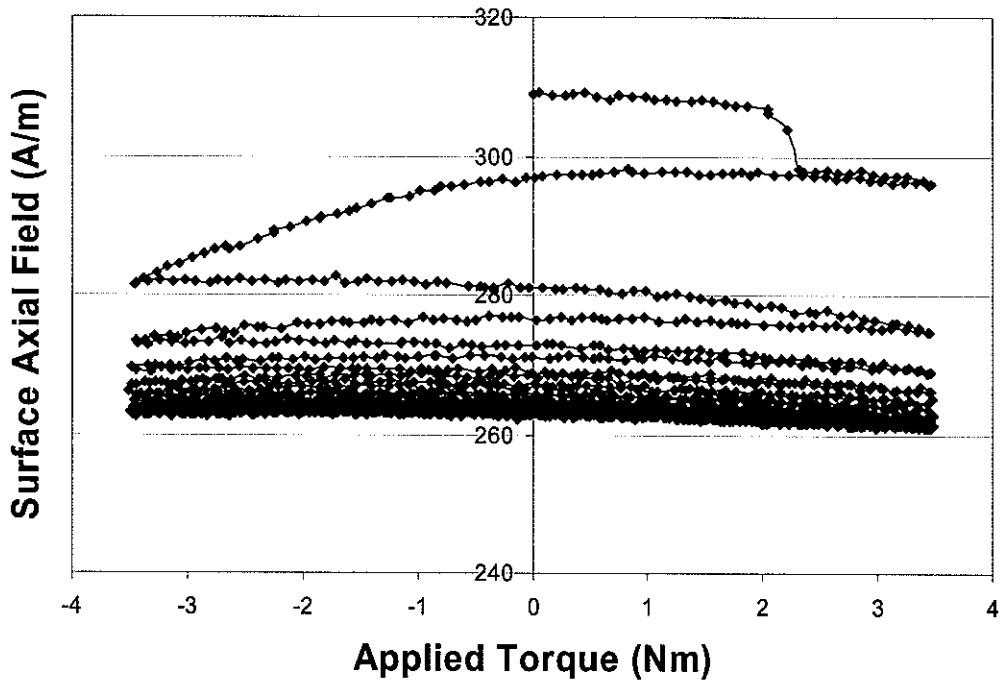


**Fig. 6.9** Magnetomechanical response of $Fe_{64}Ni_{36}$.

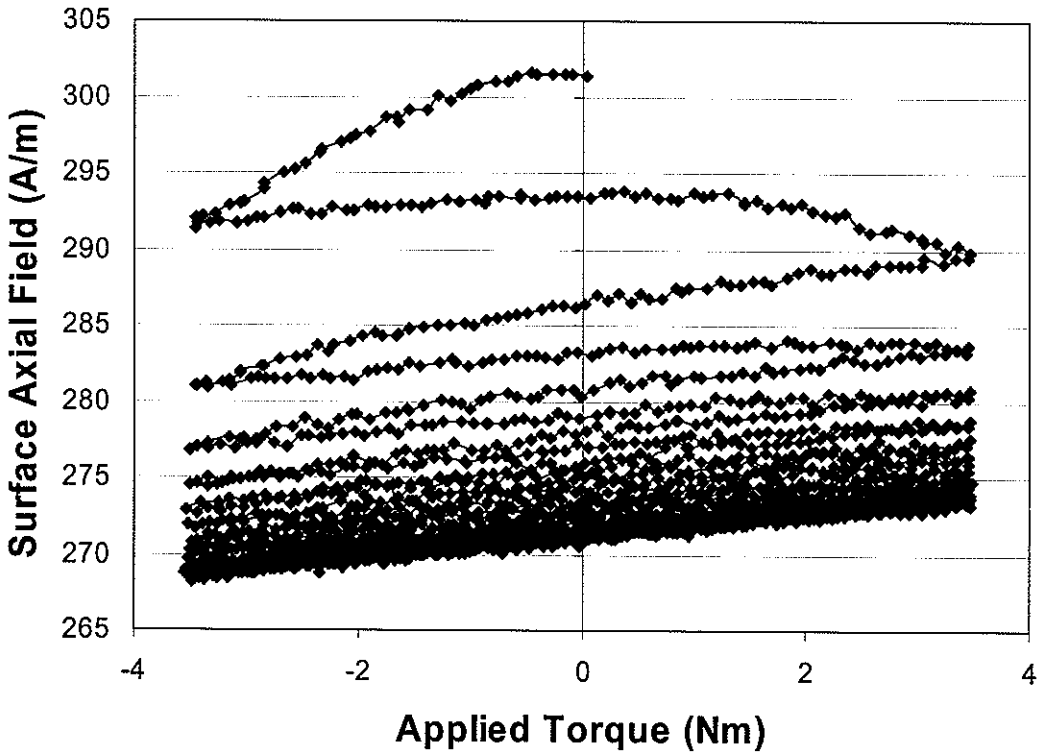


**Fig. 6.10** Magnetomechanical response of $Fe_{55}Ni_{45}$.

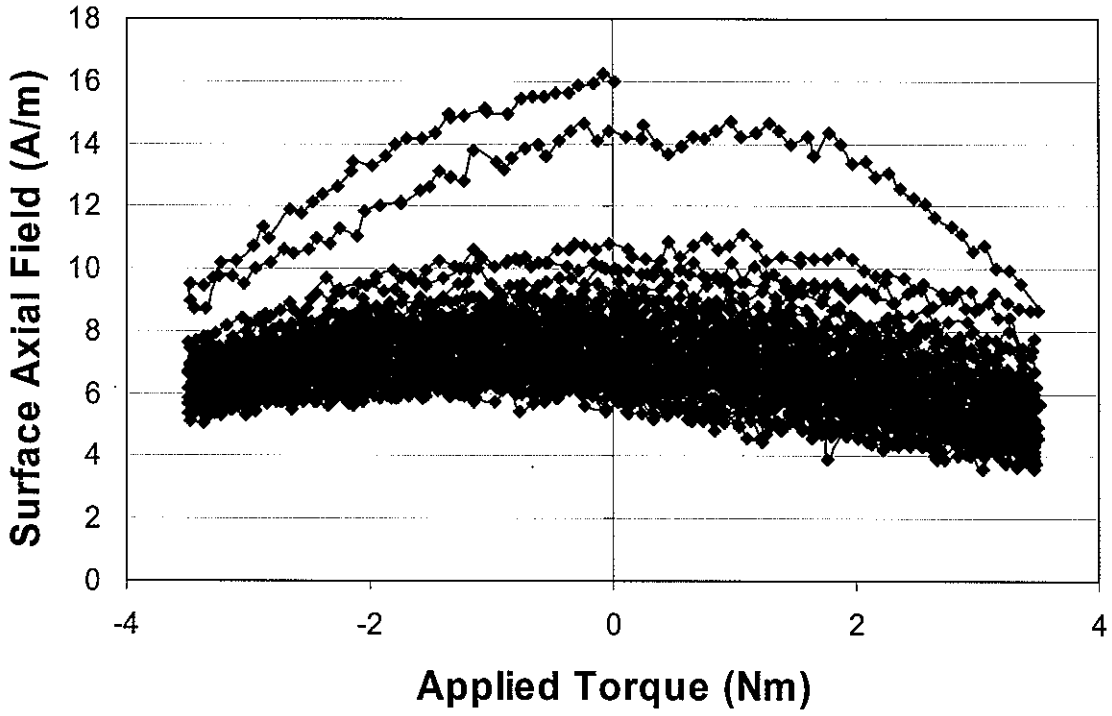


**Fig. 6.11** Magnetomechanical response of $Fe_{10}Ni_{90}$.

# Chapter 7. Discussion

## 7.1 Equilibrium behavior—factors related to sensitivity.

We shall now examine the factors that affect the of Matteucci effect. As is consistent with previous references [7, 8], we consider a quantity—magnetomechanical sensitivity—which is defined as the change of magnetic induction of a ferromagnetic sample under torque. According to thermodynamics [15], one has the following relationship in equilibrium for small amplitude of stress or field applied to ferromagnetic materials,

$$\left(\frac{dB}{d\sigma}\right)_H = \left(\frac{d\lambda}{dH}\right)_\sigma \tag{7.1}$$

where B is the magnetic induction, $\sigma$ is the stress, $\lambda$ is the magnetostriction coefficient and H is the applied magnetic field. The latter can be expressed as

$$\left(\frac{d\lambda}{dH}\right)_\sigma = \left(\frac{d\lambda}{dM}\right)_\sigma \left(\frac{dM}{dH}\right)_\sigma \tag{7.2}$$

where $M$ is the magnetization of the sample. It is well known that

$$\left(\frac{dM}{dH}\right)_{\sigma->0} = \mu_r - 1 \tag{7.3}$$

where $\mu_r$ is the relative permeability which is easily measured in experiments. In the next step, one would like to evaluate term $\left(\frac{d\lambda}{dM}\right)_{\sigma->0}$. We will consider an ideal sample with isotropic magnetostriction by which the properties of polycrystalline materials, such as nickel, are approximately approached. The average bulk magnetostriction $\lambda$ is given by,

$$\lambda=(3/2)\,\lambda_s(<\cos^2\theta>-1/3) \tag{7.4}$$

where $\lambda_s$ is the saturation magnetostriction constant, $\theta$ is the angle between the magnetization and the direction of measurement and "< >" denotes the average value. For a single crystal that contains only a single magnetic domain, the magnetization M can be expressed as,

$$M=M_s \cos\ \theta \tag{7.5}$$

where $\theta$ is the angle of $M_s$ to the direction of measurement. For multi-domain samples, along the direction of measurement we get the magnetization on average,

$$M=M_s <\cos\ \theta> \tag{7.6}$$

where $M_s$ is the saturation magnetization and $\theta$ is the angle between the direction of magnetization measured and the direction of that domain. Therefore, the sensitivity expression becomes

$$\left(\frac{dB}{d\sigma}\right)_H = \left(\frac{d\lambda}{dH}\right)_\sigma = \left(\frac{d\lambda}{dM}\right)_\sigma \left(\frac{dM}{dH}\right)_\sigma = \frac{3\lambda_s(\mu_r - 1)}{2M_s} \frac{d<\cos^2\theta>}{d<\cos\theta>} \tag{7.7}$$

Thus the stress sensitivity is related to 4 factors:

1. Configuration of domains (by the term $\frac{d<\cos^2\theta>}{d<\cos\theta>}$)
2. Relative permeability $\mu_r$
3. Saturation magnetostriction constant $\lambda_s$
4. Saturation magnetization $M_s$.

The first factor describes how the configuration of magnetic domains affects the magnetomechanical sensitivity. For example, when a nickel rod under torque with different initial conditions, such as demagnetized status, remanence status along the axis or remanence

along the circumference, the magnetic induction near the surface along the axis is totally different. For a single magnetic domain, since

$$\frac{d\cos^2\theta}{d\cos\theta} = 2\cos\theta \tag{7.8}$$

the smaller the angle between the direction of measurement and the magnetization, the larger value of $\frac{d\cos^2\theta}{d\cos\theta}$. Thus one would expect the largest $\frac{d\lambda}{dM}\left(\propto \frac{d\cos^2\theta}{d\cos\theta}\right)$ near saturation magnetization $M_s$, according to reference [27].

The second factor—relative permeability $\mu_r$—indicates that both domain wall movement and domain rotation affect the sensitivity. The expression developed by Garshelis [2], Herbst [6] and Chen [8] do not include the contribution of domain wall movement to the sensitivity of magnetomechanical effect. In those expressions, only the mechanism of magnetic domain rotation was considered. The magnetization in the domains was supposed only to rotate under the influence of stress and magnetocrystalline anisotropy. We shall see in the next section that this is not the case. Actually, the magnetic domain wall movement plays the main role for a high sensitivity in most cases. Sablik and Jiles [27] discussed the difference between the domain wall movement mechanism and the domain rotational mechanism of a ferromagnetic composite rod under torsion.

### 7.2 Magnetomechanical mechanism in nickel

The effect of torsional stress on magnetization was modelled by Sablik and Jiles [29]. A torsional stress can be decomposed to 2 perpendicular surface stresses, as shown in Fig.5.2. There exists an energy associated with the magnetization and stress. Consider the positive tensile stress $\sigma$. The energy raised by this stress to the magnetization can be simply presented as [15],

$$E_\sigma = -\frac{3}{2}\sigma\lambda = -\frac{3}{2}\sigma\lambda_s \cos^2\theta \tag{7.9}$$

where $\sigma$ is the applied stress along the positive stress direction, $\lambda_s$ is the saturation magnetostriction of the sample and $\theta$ represents the angle between the local magnetization and the positive stress axis. By the same reasoning, the energy raised by the compressive stress is given by,

$$E_{-\sigma} = -\frac{3}{2}(-\sigma)\lambda = -\frac{3}{2}(-\sigma)\lambda_s \sin^2\theta \tag{7.10}$$

The total energy raised by the two stresses is given by the sum of the above two energies,

$$E_\sigma = E_{-\sigma} + E_\sigma = -\frac{3}{2}\sigma\lambda_s \cos(2\theta) \tag{7.11}$$

Let's only consider the magnetic domain rotation under torque, which results from the competition between magnetocrystalline anisotropy energy and the magnetoelastic energy. For nickel sample, if the deviation of magnetization from the easy direction is small, the energy raised by this deviation can be represented by,

$$E_k = -K_1 \sin^2\alpha \tag{7.12}$$

where $\alpha$ is the deviation of magnetization from the <111> easy direction of the magnetocrystalline anisotropy. The relationship of $\theta$ and $\alpha$ is illustrated in Fig. 7.1. It can be seen that the change of $\theta$ is the same of the change of $\alpha$ for nickel.

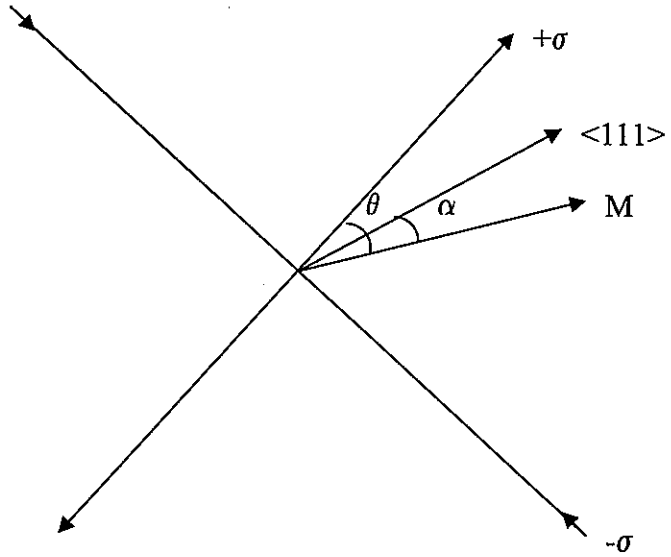


**Fig. 7.1.** Illustration of the angles among the pull stress, magnetization and the easy direction of magnetocrystalline anisotropy of nickel rod.

According to the least energy principal at equilibrium and bearing in mind that $d\theta = d\alpha$, we get

$$\frac{d(E_\sigma + E_k)}{d\theta} = -\frac{3}{2}\sigma\lambda_s \frac{d\cos(2\theta)}{d\theta} - K_1 \frac{d\sin^2\alpha}{d\alpha} = 3\sigma\lambda_s \sin(2\theta) - K_1 \sin(2\alpha) = 0 \tag{7.13}$$

This gives,

$$\sin(2\alpha) = \frac{3\sigma\lambda_s}{K_1}\sin(2\theta) \tag{7.14}$$

For a rod under torque, the decomposed perpendicular stress $\sigma$ from the rod axis at a radial distance r is related to the torque $\tau$ by

$$\sigma(r) = 2\frac{Tr}{\pi R^4} \text{ and } \sigma(R) = \frac{2T}{\pi R^3} \tag{7.15}$$

where R is the radius of the cylinder, T is the torque applied on the cylinder. In our experiments, R=12.7 mm. Consider the typical maximum torque we employed—3.5Nm—which corresponds to $\sigma_{\max}(R) = 8.1\,\text{MPa}$. And $\lambda_s = -34\times10^{-6}$; $K_1 = 5\times10^3 Jm^{-3}$. Using these values of $\sigma$, $\lambda_s$ and $K_1$, we can estimate the rotation angle of magnetization from the easy magnetocrystalline direction from equation (7.14).

$$\left|\sin(2\alpha)\right| = \left|\frac{3\sigma\lambda_s}{K_1}\sin(2\theta)\right| \le \left|\frac{3\sigma\lambda_s}{K_1}\right| = 0.17, \qquad \alpha_{\max} = 4.8^\circ \tag{7.16}$$

this small angle is not enough to cause irreversible domain rotation even for cubic crystal anisotropy with <111> easy direction which needs at least 35.3° to make this change. It means that most of the irreversible magnetomechanical response comes from the magnetic domain wall movement. Therefore, to decrease the hysteresis, it is better to employ more mechanism of domain rotation than mechanism of domain wall movement.

Now we shall demonstrate that the mechanism of magnetic domain wall movement rather than that of magnetic domain rotation plays the main role in this Matteucci effect process. Expression (7.12) gives the equivalent magnetic field due to magnetocrystalline anisotropy by

$$H_k = \frac{dE_k}{\mu_0 dM} \tag{7.17}$$

where $\mu_0$ is the vacuum permeability. The magnetization component of a single domain along the easy magnetocrystalline direction <111> is given by

$$M = M_s \cos\alpha \tag{7.18}$$

Combining equation (7.12), (7.17) and (7.18), we get,

$$H_k = -\frac{K_1 \sin(2\alpha)}{\mu_0 M_s} \tag{7.19}$$

Bearing in mind that $\alpha_{\max} = 4.8^\circ$ (expression (7.16)), we get,

$$\left|H_k\right|_{\max} = \left|-\frac{K_1 \sin(2\alpha)}{\mu_0 M_s}\right| = \left|-\frac{5\times10^3 \times \sin(4.8^\circ)}{4\pi\times10^7 \times 4.84\times10^5}\right| = 616 \quad A/m \tag{7.20}$$

We shall see that this is a very small value compared to the equivalent field due to torque.

Expression (7.11) gives the equivalent magnetic field due to the torque by

$$H_\sigma = \frac{dE_\sigma}{\mu_0 dM} \tag{7.21}$$

where $\mu_0$ is the vacuum permeability. Using the results of (7.11) and (7.21), we get,

$$H_\sigma = -\frac{3}{2\mu_0}\lambda_s\left(\cos 2\theta \left.\frac{d\sigma}{dM}\right|_H + \sigma\frac{d\cos 2\theta}{dM}\right) \tag{7.22}$$

The magnetization component of a single domain along the tensile stress direction is given by

$$M = M_s \cos\theta \tag{7.23}$$

Combining equation (7.22) and (7.23), we get,

$$H_\sigma = -\frac{3}{2\mu_0}\lambda_s\left(\cos 2\theta \frac{d\sigma}{dM}\bigg|_H + \frac{4\sigma\cos\theta}{M_s}\right) = -\frac{3}{2}\lambda_s\left(\cos 2\theta \frac{d\sigma}{dB}\bigg|_H + \frac{4\sigma\cos\theta}{\mu_0 M_s}\right) \tag{7.24}$$

To experimentally evaluate expression (7.24), we measured the change of the magnetic induction of a nickel rod under tensile and compressive stress when the rod is at remanence status (Fig. 6.4). The experimental value of $\frac{\mathrm{d}\sigma}{\mathrm{dB}}$ near the remanence status is $5\times10^{8}\, Nm^{-2}T^{-1}$.

We obtain the maximum equivalent magnetic field due to the torque,

$$|H_\sigma|_{\max} = \left|-\frac{3}{2}\times(-34)\times10^{-6}\times(5\times10^{8}) + \frac{4\times(8.1\times10^{6})}{(1.26\times10^{-6})\times(4.84\times10^{5})}\right| = 5.3\times10^{7}\ A/m \tag{7.25}$$

compared to the typical coercitivity of 400 A/m and saturation field of 20 kA/m [15] for nickel, this equivalent magnetic field is really large. If the magnetic domain rotation mechanism played the important role, the effective magnetic field in equation (7.25) would be almost the real magnetic field which makes the magnetization to saturation. However the experimental data (Fig. 6.3) demonstrate that this is not the case. This means the mechanism of domain wall movement rather than the magnetic domain rotation occurred mainly in the process.

As direct experimental evidence, after 15 cycles of torque, we measured the sensitivity change against temperature as shown in Fig 6.5. It can be seen that the sensitivity decreases 20% when the temperature goes from -20 °C to 80 °C. On the other hand, the quotient $\frac{\lambda_s}{K_1}$ almost does not change [16]. This disagrees with the theoretically predicted linear sensitivity from magnetic domain rotation developed by both Herbst [6] and Garshelis

[2,3] which is approximately proportional to $\frac{\lambda_s}{K_1}$. The observed 20% sensitivity change with temperature suggests that the torque sensitivity of the nickel rod mainly comes from the mechanism of domain wall movement which is temperature dependent. The sensitivity drops as temperature increases because when the temperature increases, the weakly pinned domain walls is released. At new equilibrium position, the pinning of domain wall is much stronger than before, so the potential energy varies much faster than before. It requires more energy to overcome this pinning. Thus the sensitivity drops as temperature increases. The experimental results by Chen (Fig.1.2) also agree to our experiment data.

### 7.3 Dynamic process of the Matteucci effect in nickel, iron and cobalt

The spatial illustrations of the relative magnitude of magnetoelastic energy are drawn as Fig. 7.1 according to the expression (7.11). It can be seen that the two perpendicular stress axes are the highest energy directions alternately when the stress cycle alternates (i.e. when the applied torque changes from CW to CCW or vice versa). From the experimental data shown in Fig. 6.3, it is reasonable to propose that, for the as-fabricated nickel sample, after 15 cycles of torque, most of the magnetic domains near the directions of the two stress axes were incorporated into the magnetic domains near the horizontal and perpendicular directions. This process causes the drop of the magnetization along the sample axis as shown in Fig. 6.3. The final linear magnetomechanical response mainly comes from the mechanism of magnetic domain wall movement among the domains near these two directions. Since the nickel rods are magnetized along the cylindrical axis to get remanence status before running the test, it is reasonable that the magnetic domains oriented with magnetization in the upper hemisphere

directions dominate against those oriented with magnetization in the lower hemisphere. Since the initial torque in CW and CCW will cause the favoring of domain directions along left and right, this causes the initial direction dependence of the Matteucci effect of the as-fabricated nickel rods as shown in Fig. 6.3.

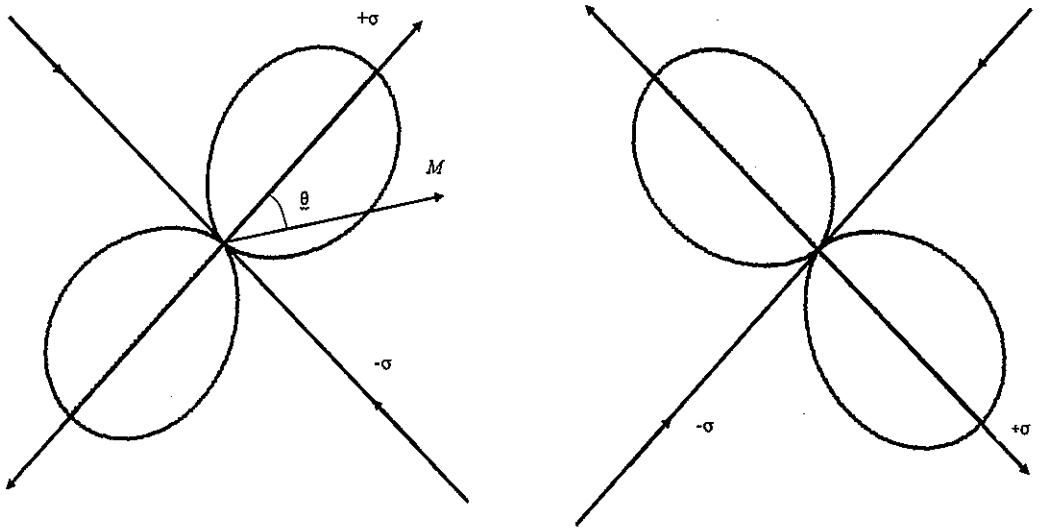


(a) Torque in CW direction. (b) Torque in CCW direction.

**Fig. 7.2** Illustration of the relative magnitude of magnetoelastic energy under torque in (a) CW and (b) CCW direction. The radial length of the curve presents the magnitude of magnetoelastic energy due to torque.

It is interesting that after annealing the nickel sample at 500 °C for 2 hours, the Matteucci effect is totally different. These results are shown in Fig. 6.6 and Fig. 6.7. After annealing, the permeability of nickel increased and the pinning of domain walls was greatly released. Thus the torsional stress within the range of our experiments is large enough to allow most of the high energy domains to be incorporated into the lowest energy domain. In every cycle of torque, the high energy stress axis and low energy stress axis change position.

Magnetic domains favorite these two axes alternately expand and retract volume accordingly. The magnetic domain wall movement mainly occurred between domains near these two axes. In this case, as shown in Fig 6.6 and Fig 6.7 a linear response of magnetization can no longer be obtained.

The magnetomechanical response of iron to applied torque shown in Fig. 6.1 can be explained for the same reasons. The magnetization almost does not change for the cobalt rod within the torque range of our experiment (Fig. 6.2). This is because cobalt has large magnetocrystalline anisotropy and thus a large coercivity. Thus the effect of stress is too weak to make much magnetic domain rotation and magnetic domain wall movement.

### 7.4 Matteucci effect in nickel rod magnetized along the axis and nickel ring magnetized along the circumference

Much attention has been paid to a magnetically polarized ring along circumference since Garshelis developed a prototype of non-contact torque sensor based on this method in 1992 [2]. The obvious advantage of this method is that a linear signal (magnetization) against torque can be obtained with small stress. For engineering applications, it is always interesting to increase the sensitivity of a torque sensor. A high sensitivity material—cobalt ferrite composite—has been developed based on this method. However, our further experimental result shows that at least in the interest of sensitivity it is not best to magnetically polarize a ring circumferentially.

Fig. 6.8 shows the magnetomechanical response of a nickel ring. The ring was magnetized to saturation along the circumference before the test and a Hall sensor was put near the surface to record the magnetic induction change along the axis. The best results of

the sensitivity we have obtained is 4.7 (A/m)/(Nm) (Fig. 6.8). However, the sensitivity of all the as-fabricated nickel rods after 15 cycles, i.e. Fig. 6.3, is between 11~35 (A/m)/(Nm). It is reasonable to suppose that the mechanism of magnetic domain rotation plays a more important role in the nickel ring than that in nickel rod because of the different initial magnetic status. This suggests that to get a high sensitivity torque sensor, one should employ more of the mechanism of domain wall movement rather that domain rotation.

### 7.5 Experimental results on permalloy

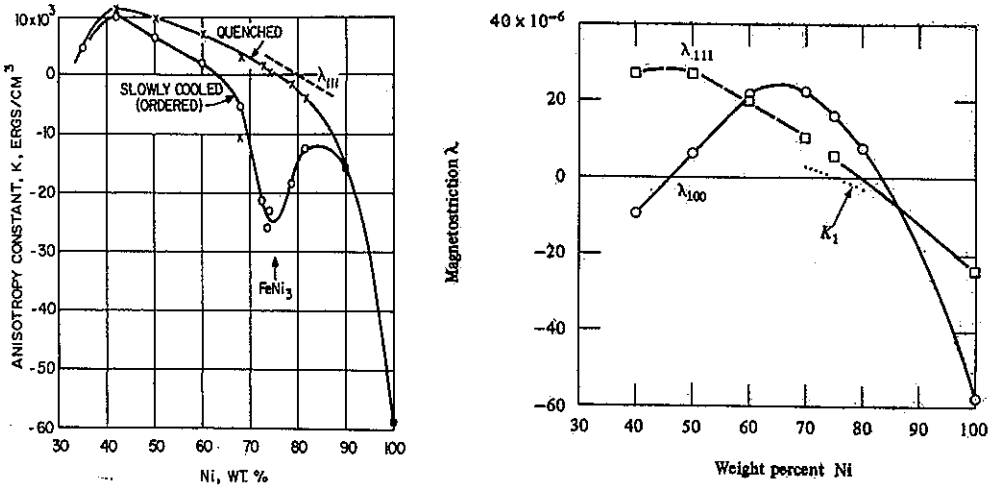


**Fig. 7.2** Composition dependence of anisotropy constant and magnetostriction λ of iron nickel alloys, after Bozorth [25] and Jiles [15].

As stated in the previous sections, the magnetic domain wall motion plays an important role in high sensitivity materials. Since there is a rich variation of magnetic domain movement in iron and nickel alloy, we shall now examine the magnetomechanical response of permalloy. Our objective was to find a linear response with high sensitivity in permalloy.

Fig 6.9, Fig 6.10 and Fig 6.11show the Matteucci effect of $Fe_{10}Ni_{90}$, $Fe_{55}Ni_{45}$ and $Fe_{64}Ni_{36}$. Unfortunately, only in $Fe_{55}Ni_{45}$ was there a linear response of the magnetization

along the axis. Furthermore the sensitivity was lower than that of as-fabricated nickel. Fig.7.2 shows the compositional dependence of anisotropy constant and magnetostriction λ of permalloy. It seems that a linear and high sensitivity is expected for those materials with high quotient $\frac{\lambda_s}{K}$, high K and low coercivity (high permeability).

## 7.6 Conclusions

The Matteucci effect in iron, cobalt, nickel and permalloy rods has been documented when they were in magnetic remanence status along the axis and nickel ring when they were in remanence status along the circumference. The effect of annealing on the magnetomechanical effect in nickel and the temperature dependence of the magnetomechanical sensitivity has also been examined.

Factors related to the sensitivity at equilibrium condition have been theoretically developed. It is found in the experiments that the mechanism of magnetic domain wall movement plays an important role rather than the domain rotation. A higher sensitivity was found by domain wall movement mechanism than that by domain rotation mechanism. However, the domain wall movement will result in more hysteresis than domain wall rotation.

The dynamic process of Matteucci effect of iron, cobalt, permally, especially as-fabricated and annealed nickel rods have been examined. A tentative explanation for the difference of these in terms of magnetic domain configuration and movement was given.

As a result, another method of configuring and processing magnetic domains to get a linear magnetomechanical response other than that suggested by Garshelis [2], which was the basic method before the present studies, has been experimentally developed and theoretically

analyzed. A higher sensitivity was obtained in nickel by employing this method than that by employing the method of Garshelis. The results suggest that magnetic domain configuration is very important in designing a high sensitivity magnetic torque sensor.

## References


1. C. Heck, "Magnetic materials and their applications", Crane, Russak, New York, 1974. Ch. 1.
2. I. Garshelis, "A Torque Transducer Utilizing a Circularly Polarized Ring", IEEE Trans. Mag. **28**, 2202, 1992.
3. I. Garshelis, and C.R. Conto, "A magnetoelastic torque transducer utilizing a ring divided in two oppositely polarized circumferential regions", J. Appl. Phys., **79**(8), 4756, 1996.
4. I. Garshelis, and C.A. Jones, "A torque transducer based on local bands of naturally stabilized remanent circumferential magnetization", J. Appl. Phys., **85**(8), 5468, 1999.
5. D. C. Jiles, "Theory of the magnetomechanical effect", J. Phys. D: Appl. Phys., **28** 1537 (1995).
6. J.F. Herbst and F.E. Pinkerton, "Model Calculations of torque-induced axial magnetization in circumferentially magnetized rings: small angle approximation", J. Magn. & Magn. Mat. **176**, 183, 1997.
7. Y. Chen, J.E. Snyder, K.W. Dennis. R.W. McCallum and D.C. Jiles, "Temperature dependence of the magnetomechanical effect in metal-bonded cobalt ferrite composites under torsional strain", J. Appl. Phys., **87**(9), 5798, 2000.
8. Y. Chen, B. K. Kriegermeier-Sutton, J. E. Snyder, K. W. Dennis, R. W. McCallum and D. C. Jiles. Journal of Magnetism and Magnetic Materials **236**, (2001) 131-138.
9. E.J. Hearn, "Mechanics of Materials", Pergamon Press Ltd, New York, 1977.

10. CRC Handbook of Chemistry and Physics, Robert C. Weast, Ed. 62 Edition, CRC Press, Boca Raton, FL, 1981.

11. Metallic Materials Specification Handbook, Fourth Ed., Robert B. Ross, Chapman & Hall, London, 1992.

12. Metals Handbook, Vol.2 - Properties and Selection: Nonferrous Alloys and Special-Purpose Materials, ASM International 10th Ed. 1990.

13. The Metals Databook, Alok Nayer, McGraw-Hill, New York, 1997.

14. Y. C. Fung, "A first course in continuum mechanics". N.J. Prentice-Hall, Englewood Cliffs, c1977.

15. D. C. Jiles, "Introduction to Magnetism and Magnetic Materials", Second Edition, Chapman & Hall, New York, 1998.

16. B.D. Cullity, "Introduction to Magnetic Materials", Addison-Wesley Publishing Comp, Inc. 1972.

17. N.S. Akulov, 1928, Z. Phys., **52**,389.

18. C.S. Schneider and J.M. Richardson 1982 "Biaxial magnetoelasticity in steels," J. Appl. Phys. **53,** 8136.

19. C.S. Schneider and E.A. Semken 1981 Vibration induced magnetization. J. Appl. Phys. **52,** 2425.

20. C.S. Schneider P.Y. Cannell and K.T. Watts 1992 Magnetoelasticity for large stresses IEEE Trans. Magn. **28,** 2626.

21. M. J. Sablik and D.C. Jiles 1993 "Coupled magnetoelastic theory of magnetic and magnetostrictive hysteresis," IEEE Trans. Magn. **29,** 2113.

**22.** Trémolet de Lacheisserie, Etienne du, "Magnetostriction: Theory and Applications of Magnetoelasticity", CRC Press, Boca Raton, FL, USA, 1993.

**23.** E.W. Lee, "Magnetostriction and Magnetomechanical Effects". Reports on Prog. In Phys., **18**, 184-220 (1955).

**24.** R.R. Birss, "The Saturation Magnetostriction of Ferromagnetics", Advances in Physics., **8**, 252-291 (1959).

**25.** R.M. Bozorth, (1951) Ferromagnetism, Van Nostrand, New York.

**26.** Trémolet de Lacheisserie, Etienne du. "Magnetostriction : theory and applications of magnetoelasticity" Boca Raton : CRC Press, c1993.

**27.** D.C. Jiles, T.T. Chang, D.R. Hougen and R. Ranjan. "Stress-induced changes in the magnetic properties of some nickel-copper and nickel-cobalt alloys". J. Appl. Phys., **64** (1988), 3620.

**28.** M.J. Sablik and D.C. Jiles, "A modified Stoner-Wohlfarth computational model for hysteretic magnetic properties in a ferromagnetic composite rod under torsion". J. Phys. D: Appl. Phys. **32,** 1971, (1999).

**29.** M.J.Sablik and D.C.Jiles, "Modeling the effects of torsional stress on hysteretic magnetization", IEEE Transactions on Magnetics, **35**, 498, (1999).

## Acknowledgements

I am greatly indebted to my major professor Dr. David C. Jiles for his academic guide and encouragement of this study.

I would like to thank Dr. John E. Snyder and Dr. Chester C.H. Lo for their help and very useful discussion. Many thanks go to Dr. Gary Tuttle for dedicating time to serve on my committee.

I also want to express my thanks to Andy Ring, Jason Paulsen, Bryan Baker, Toshikazu Kawaguchi and Nanlin Wang for their kindly help in the experiments.

This work was supported by the National Science Foundation, Division of Materials Research, under grant number DMR-9902415 and the Ames Laboratory under Contract No. assigned the DOE Report number IS-T 2296 to this thesis.